Lithos 342–343 (2019) 295–314

Contents lists available at ScienceDirect

Lithos

journal homepage: www.elsevier.com/locate/lithos

Metamorphic devolatilization of basalts across the greenschist-amphibolite facies transition zone: insights from isograd mapping, petrography and thermodynamic modelling

Starr Paul G. *,[1], Pattison David R.M.

Department of Geoscience, University of Calgary, 2500 University Drive NW, Calgary, AB T2N 1N4, Canada

ARTICLE INFO

Article history:
Received 7 March 2019
Received in revised form 14 May 2019
Accepted 17 May 2019
Available online 22 May 2019

Keywords:
Orogenic gold deposits
Metamorphic devolatilization
Metamorphic fluids
Greenstone belts
Greenschist facies
Amphibolite facies

ABSTRACT

The greenschist-amphibolite facies transition zone within metabasites is of great importance due to the common occurrence of this transition within greenstone belts, and the proposition that fluids released across the transition may be involved in orogenic gold deposit formation. In this work, the nature of devolatilization reactions occurring across the greenschist-amphibolite facies transition zone is assessed from petrological examination and thermodynamic modelling of an exceptionally exposed part of the Flin Flon Greenstone Belt (Manitoba/Saskatchewan). The sequence at Flin Flon comprises an intact metamorphic sequence of ~10 km length spanning the greenschist and lower amphibolite facies, the latter of which can be subdivided into three zones (from S to N): the hornblende-actinolite zone, the hornblende-actinolite-oligoclase zone, and the hornblende-oligoclase zone, demarcated by the hornblende-in, oligoclase-in and actinolite-out isograds. The crossing of the hornblende-in isograd is associated with small amounts of hornblende growth, relatively little change in the proportions of chlorite, and negligible fluid loss. By contrast, significant changes in the modal mineralogy occur across the 1500 m wide hornblende-actinolite-oligoclase zone, with the breakdown of approximately 75% of the chlorite and the loss of approximately 1-2 wt% H_2O. There is no textural or modal evidence for significant loss or gain of carbonate or sulphide minerals going through this interval. Petrological estimates of devolatilization across the greenschist-amphibolite facies transition zone are compared with predictions from thermodynamic modelling. Although there are differences between the two, both indicate that the fluid loss is strongly tied to variation in bulk composition, the latter predominantly the result of pre-metamorphic alteration processes. High-Mg and high-Ca basalts, representative of pillow rim and core material, undergo an average of 1.8 wt% (modelling estimate: 2.2 wt%) and 1.1 wt% H_2O loss (modelling estimate: 1.8 wt%), respectively, across the hornblende-actinolite-oligoclase zone. T-XCO_2 modelling predicts that the XCO_2 content of fluid produced from the hornblende- and oligoclase-producing reactions is low (<0.08) and is not buffered to higher XCO_2 compositions, consistent with the lack of carbonate breakdown documented within the Flin Flon sequence over this interval. Fluid buffering path modelling predicts significant volumes of fluid release with higher XCO_2 contents (>0.2) above the greenschist-amphibolite facies transition zone within samples containing high carbonate contents (>5%). However, in contrast to the modelling, the majority of chlorite (>75%) breaks down at the main greenschist-amphibolite facies transition zone in the Flin Flon sequence, and most samples have low carbonate contents (1.5% average), limiting the volumes of fluids with higher XCO_2 compositions that can be generated at higher grades. Thus, whilst the greenschist-amphibolite facies transition zone at Flin Flon is the site of significant devolatilization (1-2 wt%) over a small interval of P-T space, is does not appear to have been accompanied by significant carbonate and sulphide breakdown, and the fluids generated across this interval were CO_2-poor. If the Flin Flon sequence is representative of other metamorphosed greenstone belts, it may be that metabasites metamorphosed across the greenschist-amphibolite facies transition zone do not, in general, release the CO_2– and gold hydrosulphide-bearing fluids characteristic of orogenic gold deposits.

1. Introduction

The transition zone between greenschist and amphibolite facies assemblages within metabasalts is one of the most important metamorphic facies boundaries due to its widespread development, especially

* Corresponding author.
E-mail address: starrp@bc.edu (P.G. Starr).
[1] Authors Current Address: Department of Earth and Environmental Sciences, Boston College, 140 Commonwealth Avenue, Chestnut Hill, Massachusetts, 02467, USA.

https://doi.org/10.1016/j.lithos.2019.05.020
0024-4937/

in greenstone belts, and its association with a number of major devolatilization reactions. The greenschist-amphibolite facies transition zone has attracted particular interest due to its common association with orogenic gold deposits and the proposed link between the fluids generated across the transition and the source fluids for orogenic gold deposits (e.g. Elmer et al., 2006; Goldfarb et al., 2005; Goldfarb and Groves, 2015; Kerrich and Fyfe, 1981; Phillips and Powell, 2009, 2010, 2011; Powell et al., 1991; Tomkins, 2010, 2013). Based on geological and geochemical observations from orogenic gold deposits, it has been suggested that a fluid source for orogenic gold formation should be capable of producing large volumes of fluids with dissolved Au in the form of hydrosulphide complexes (e.g. $Au(HS)_2^-$ and AuHS) and mixed H_2O-CO_2 compositions with moderate XCO_2 contents (e.g. ~0.2–0.3) (e.g. Elmer et al., 2006; Goldfarb and Groves, 2015; Kerrich and Fyfe, 1981; Phillips and Evans, 2004; Pitcairn et al., 2006; Powell et al., 1991; Tomkins, 2010, 2013). Thus, in the case of a metamorphic devolatilization model, fluid production should coincide with sulphide and carbonate breakdown in order to produce the expected fluid compositions (e.g. Elmer et al., 2006; Powell et al., 1991; Tomkins, 2010, 2013).

This study focuses on an exceptionally exposed greenschist-amphibolite facies transition zone located in the Flin Flon Greenstone Belt in Manitoba and Saskatchewan. A number of features make the Flin Flon area an ideal natural laboratory for the detailed characterization of the metamorphic evolution of greenschist and lower amphibolite facies metabasalts: (1) the excellent exposure, including almost 100% exposure across much of the area covering the greenschist-amphibolite facies transition; (2) the well-defined volcanic stratigraphy and field relations; (3) recognition and mapping of pre-metamorphic hydrothermal alteration (Ames et al., 2016; this study); and (4) the lack of significant post-metamorphic deformation that might complicate the metamorphic sequence.

This study provides the first detailed field-based examination of devolatilization within metabasites across the greenschist-amphibolite facies transition zone, and provides a test of predictions made by modelling-focused studies (e.g. Elmer et al., 2006; Powell et al., 1991). The results of this study and the comparison of the natural observations with thermodynamic modelling predictions are used to assess: (1) the estimated amount and compositions of the fluid derived from the Flin Flon sequence; (2) the nature and relative importance of reactions across the transition zone; (3) the role of bulk compositional variation in controlling the evolution of metamorphic mineral assemblages; and (4) the potential for fluids generated across this metamorphic facies transition to be associated with orogenic gold deposit formation.

2. Geological background

The Flin Flon – Glennie complex (FFGC) forms part of the Trans-Hudson Orogen (THO), and straddles the border between Manitoba and Saskatchewan (Fig. 1a, b). The FFGC is composed of a collection of different accreted tectono-stratigraphic arc assemblages that form the internal part of the THO (the 'Reindeer Zone'), that separates the Archean Superior, Hearne and Sask cratons. (Fig. 1a) (Lucas et al., 1996; Stauffer, 1984; Stern et al., 1995; Syme et al., 1999). The first important tectono-metamorphic stage in the development of the FFGC involved intra-oceanic accretion of various arc-related volcanic and plutonic rocks to form the FFGC microcontinent, estimated to occur between approximately 1.92–1.83 Ga (e.g. Lucas et al., 1996; Stern et al., 1995). The second stage involves the collision of the newly accreted FFGC and a number of Archean cratonic belts, including the Sask and Superior cratons, between approximately 1.84–1.69 Ga (Ashton et al., 1999, 2005; Bickford et al., 1990; Fedorowich et al., 1995; Lucas et al., 1996).

The area around the town of Flin Flon contains a number of prolific volcanogenic massive sulphide (VMS) deposits, including the Flin Flon, Callinan and, currently active, 777 deposits (e.g. Ames et al., 2002, 2016; Syme et al., 1999). The field area for this study, shown in Fig. 1b, comprises mostly volcanic rocks of the Flin Flon arc assemblage and sediments of the Missi group. With reference to the VMS deposits, the stratigraphy may be divided into footwall and hangingwall sequences (e.g. Ames et al., 2002, 2016; DeWolfe et al., 2009; Dewolfe and Gibson, 2006). The footwall sequence consists of the Flin Flon formation and hosts the Flin Flon, 777 and Callinan VMS deposits. The overlying Hidden and Louis formations, which are composed predominantly of pillow basalts and mafic volcaniclastics, comprise the hangingwall sequence to the Flin Flon orebodies and are the main focus of this study. The broad Flin Flon domain is suggested to have undergone three main metamorphic events: an early hornblende hornfels facies stage resulting from granitoid intrusions around 1.86–1.84 Ga ($^{40}Ar/^{39}Ar$); a later regional lower greenschist to lower amphibolite regional event at 1.82–1.79 Ga ($^{40}Ar/^{39}Ar$); and a final retrograde episode dated between 1.79 and 1.69 Ga ($^{40}Ar/^{39}Ar$) (Fedorowich et al., 1995).

3. Metamorphism and alteration of the Flin Flon area - overview

3.1. Methods

Mineral compositional analyses were determined utilizing wavelength dispersive spectrometry (WDS) using a JEOL JXA-8200 electron microprobe at the University of Calgary. An acceleration voltage of 15 kV, a current of 20 nA and an approximate spot size of 5 μm were used for all spot analyses. Due to the fine grained nature of the metamorphic mineral assemblages, particularly within the matrix, a method involving combining back-scatter electron (BSE) images with x-ray compositional mapping was devised to accurately distinguish between different mineral phases. Different combinations of x-ray maps were overlain on top of BSE images in order to highlight areas of images corresponding to different minerals. These composite BSE and X-ray map images were then analysed utilizing colour intensity thresholding, using the program JMicrovision, to identify areas of the thin section corresponding to different mineralogy. Bulk compositions were then derived for these samples by combining the mineral modes and compositions. Idealized mineral compositions were used that were simplified to match the chemical system available for modelling each mineral, such as to minimize differences in the observed and model bulk and mineral compositions that may arise from the more limited model chemical systems used in some mineral activity-composition (a-X) models.

3.2. Metamorphic zones and isograds

A collection of thin sections from over 600 samples was used to construct a metamorphic isograd map for the Flin Flon area (Fig. 1b) (see supplementary information, Table S1 for sample coordinates). The sequence of metamorphic assemblages indicates a northwards increase in metamorphism from prehnite-pumpellyite facies in the southeastern part of the field area to lower amphibolite facies in the northwestern portion. Within the western portion of the field area, the metamorphic grade spans the greenschist and amphibolite facies, with the latter being subdivided into three different regional metamorphic zones (from S to N): hornblende-actinolite zone, hornblende-actinolite-oligoclase zone, and the hornblende-oligoclase zone (Fig. 1b, c). These zones are delineated, respectively, by the hornblende-in, oligoclase-in and actinolite-out isograds (Fig. 1b, c).

3.3. Hydrothermal alteration

In addition to the regional metamorphism within the Flin Flon arc assemblage, there is strong evidence for a pre-metamorphic hydrothermal alteration stage that developed at or shortly after the time of volcanism (Ames et al., 2002, 2016). Evidence for this alteration occurs both as preservation of original alteration mineralogy (Ames et al., 2002,

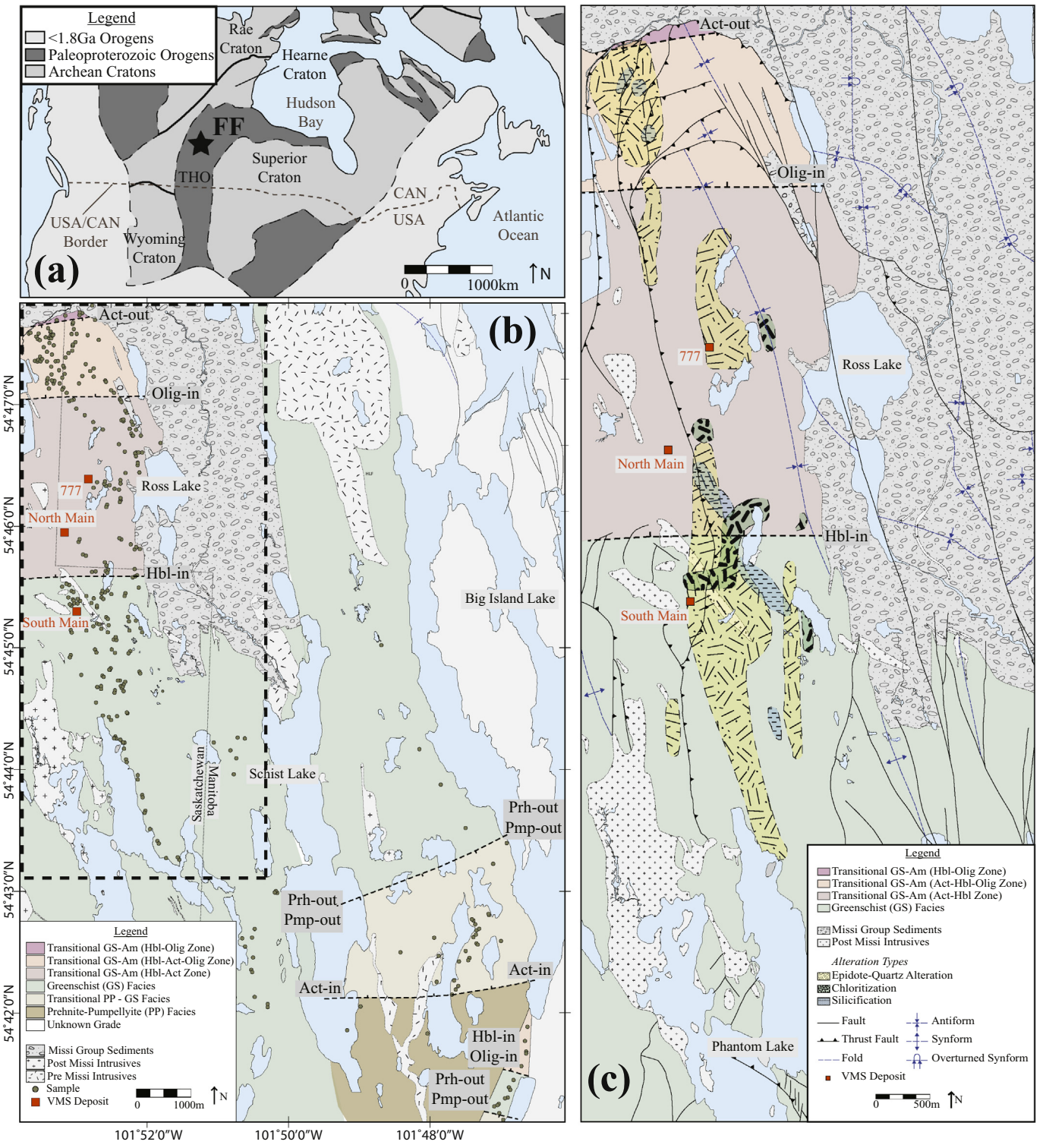

Fig. 1. Geological maps of the Flin Flon field area. (a) Simplified large scale geology map of North America showing the positioning of the major cratonic and orogenic belts. THO: Trans-Hudson Orogen. Modified after Lucas et al. (1996); originally modified from Hoffman (1988). Approximate position of the Flin Flon field area marked by star. (b) Regional metamorphic isograd map for the Flin Flon field area, superimposed on a simplified geology map. Position of Fig. 1c shown in black box. (c) Map showing spatial distribution of different alteration types (epidote-quartz, chloritization, silicification) within the hanging wall sequence. Modified from Ames et al. (2016).

2016), and as distinct geochemical signatures that influenced the later overprinting metamorphic assemblages.

The Hidden and Louis Formations, from which the majority of samples for this study were obtained, form part of the overlying hanging wall sequence to the Flin Flon orebodies and thus represent the volcanic stratigraphy deposited on top of the VMS hydrothermal system. Several types of alteration are identifiable from field and thin section observations: epidote-quartz alteration (epidotization) (Fig. 2c, d), chloritization, and silicification (Fig. 1c) (Ames et al., 2002, 2016; this study).

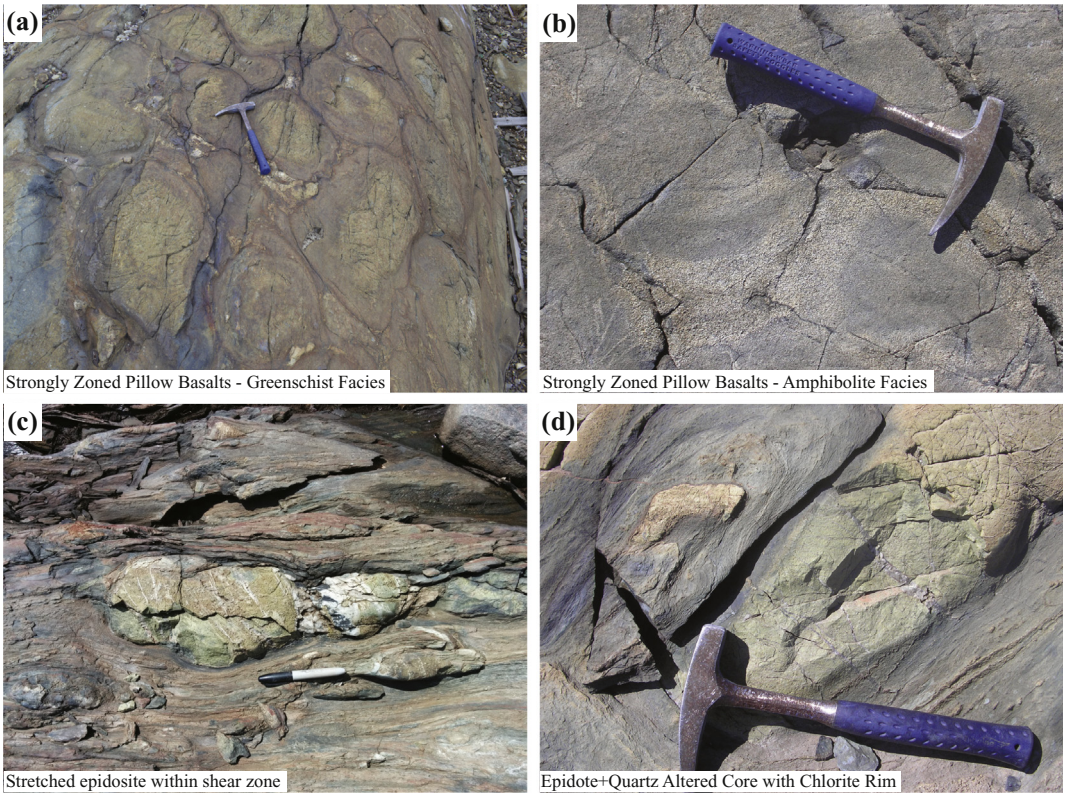

Fig. 2. Field observations of hydrothermal alteration within the Flin Flon block. (a) Altered, strongly zoned pillow basalts containing epidote-rich cores and chlorite-rich rims; (b) Strongly zoned pillow basalt at amphibolite facies, containing coarse hornblende within well defined pillow rim areas; (c) Epidosite (epidote + quartz) nodule within sheared basalts; (d) Epidotised pillow core consisting of coarser grained epidote + quartz with chlorite + amphibole dominated rim.

4. Lithologies and bulk compositional trends

Bulk compositions were acquired from 54 basaltic samples (mostly pillow basalts and basaltic dykes) spanning the greenschist and lower amphibolite facies by combining mineral compositional and modal data (see supplementary information, Table S3 for complete set of bulk compositional data). In addition, the major element bulk compositions of eight representative basaltic samples were acquired by X-ray fluorescence (XRF) at ACME Labs in Vancouver, complementing a database of 67 major and trace element bulk compositions from the Open File database of Ames et al. (2011). For comparison, bulk compositional data were collected from the literature, consisting of basaltic analyses from a range of different settings: fresh basaltic glass (Bach et al., 1994); dredged unaltered basalts (Schilling et al., 1983); altered seafloor basalts (Cann, 1969; Hart et al., 1974; Herrmann et al., 1974; Teagle and Alt, 2004), ophiolite sequences (Herrmann et al., 1974; Vallance, 1965; Wang et al., 2012) and greenstone belt sequences (Polat et al., 2003, 2007).

The bulk compositional data from the Flin Flon sequence and from the literature compilation are plotted on a CaO-Na_2O-MgO diagram (Figs. 3a, b). The ratios between these components are a useful means of distinguishing between different types of alteration (e.g. Cann, 1969; Humphris and Thompson, 1978; Widmer et al., 2000). Trends towards CaO correlate with increasing proportions of epidote (epidotization) or potentially other Ca-rich alteration minerals (e.g. prehnite, pumpellyite, grossular). Increases in MgO correlate with greater amounts of chlorite alteration (chloritization), whereas trends towards the Na_2O corner of the diagram indicate greater proportions of sodic alteration phases such as albite (spilitization). Fig. 3b shows that the bulk compositions of mafic samples within the Flin Flon sequence are highly varied, an observation ascribed to differing types and degrees of hydrothermal alteration.

Variation in composition across individual basaltic pillows from core to rim has been widely recognized to occur as a result of interaction with hydrothermal fluids at relatively low temperatures on the seafloor (e.g. Cann, 1969; Humphris and Thompson, 1978; Seyfried et al., 1978). In most cases, the rims have higher MgO and Fe_2O_3, and sometimes high MnO and K_2O, whilst the cores contain higher SiO_2 and Na_2O contents (Fig. 3a) (e.g. Humphris and Thompson, 1978; Polat et al., 2003, 2007; Seyfried et al., 1978). These trends are observed at Flin Flon where the basalts slightly more enriched in Mg are typically pillow rim compositions ('high-Mg compositions'), now represented by greater proportions of chlorite and amphibole, whilst the pillow cores are generally more enriched in Ca relative to Mg ('high-Ca compositions'), consistent with greater proportions of epidote (Fig. 3b). In coarse grained pillow basalts, this compositional variation is reflected by obvious mineralogical zoning visible in the field (Fig. 2b). This pillow basalt core-rim variation is the dominant bulk compositional heterogeneity observed in the Flin Flon sequence.

Other more minor but still volumetrically significant lithologies developed from the hydrothermal alteration of basalts include spilites and epidosites, generally attributed to higher temperature interaction of fluids with basaltic volcanics in deeper parts of the hydrothermal system, or within hydrothermal upflow zones associated with black smokers and massive sulphide deposits (e.g. Richardson et al., 1987). A number of samples from Flin Flon are characterized by high Na_2O/CaO ratios (Fig. 3b, d) and plot within the spilitic field (Fig. 3d) (after Mullen, 1983) and overlap compositionally with spilite compositions taken from the literature (Fig. 3c).

For the purpose of the following modelling discussion, the Flin Flon data are broadly divided into a number of groups: high-Mg, high-Ca and high-Na. The high-Mg compositions reflect pillow rim compositions, and are close in composition to the pillow rim compositions of Polat et al. (2003, 2007) (Fig. 3) and similar to the average MORB

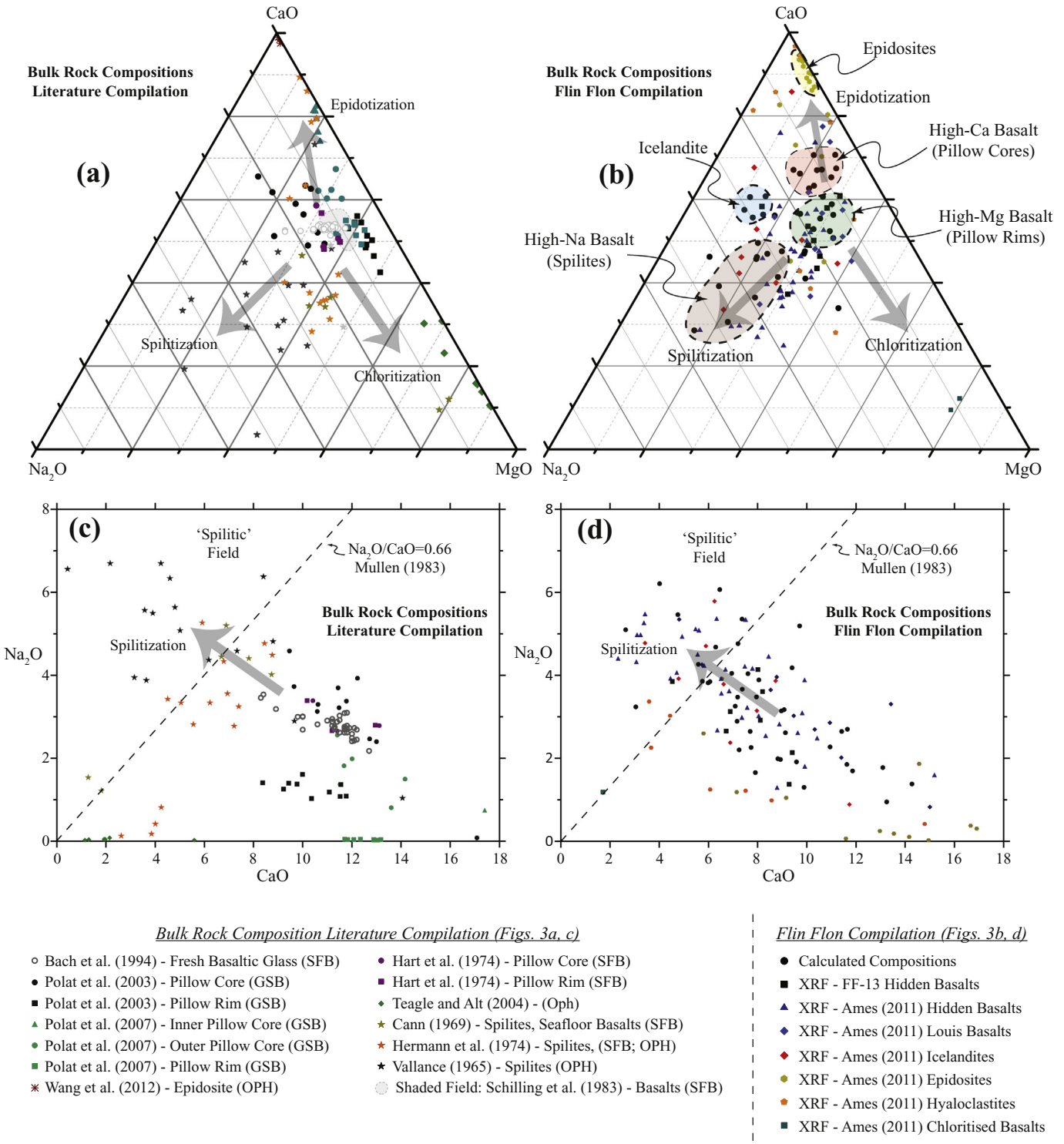

Fig. 3. Bulk compositional data for the Flin Flon sequence and a compilation of literature data. (a) and (b): CaO-Na_2O-MgO (wt%) bulk compositional diagrams for the literature compilation and the Flin Flon sequence. Arrows represent the approximate compositional vectors associated with the main alteration processes (epidotization, spilitization and chloritization). (c) and (d): Spilite compositional plots (Na_2O versus CaO – wt%) for the literature compilation and the Flin Flon sequence. SFB: Seafloor basalts. GSB: Greenstone belt. OPH: Ophiolite sequence. Compositional definition of 'spilitic' field after Mullen (1983).

compositions of Sun and McDonough (1989), though with slightly lower MgO, CaO, K_2O and TiO_2. The high-Ca and high-Na compositions reflect pillow core and spilite compositions respectively, and are representative of bulk compositions for these lithologies documented in other studies (Fig. 3).

5. Metamorphic devolatilization reactions – petrological observations

Fig. 5 shows the modal and compositional data for the Flin Flon sequence plotted along a N-S transect (used as a proxy for increasing

grade based on the location and orientation of the mapped isograds shown in Figs. 1b, c) (see supplementary information, Table S2 for modal data).

5.1. Greenschist facies

Samples within the greenschist facies are characterized by the diagnostic assemblage Act + Ab + Ep + Chl + Qtz + Ttn ± Bt ± Ms ± Stp ± Kfs ± Ap (abbreviations after Kretz, 1983). Fig. 5 demonstrates that there are no consistent trends in mineral modes or compositions going up-grade in this zone.

An evaluation of the hydrous mineral contents of the greenschist facies rocks within the Flin Flon sequence provides the starting point for determining the amount of fluid that may be released across the transition zone. Fig. 4 shows the calculated mineral-bound H_2O contents (wt %), and selected modal proportions of 26 greenschist facies samples plotted according to their bulk composition (CaO-Na_2O-MgO). The modal proportion of chlorite, which contains the majority of the mineral-bound hydrous content, varies from 4 to 24% with an average of 12.2%. The H_2O contents, which were calculated from combining the modal proportions and H_2O contents of the hydrous phases, vary from approximately 0.8 wt% to 3.8 wt% H_2O. Rocks that contain higher MgO contents are associated with greater H_2O contents as a result of higher chlorite modal proportions. By contrast, rocks with high Na_2O, interpreted to result from pre-metamorphic spilitization, are characterized by considerably lower H_2O contents.

5.2. Lower amphibolite facies: hornblende-actinolite zone

Entry into the amphibolite facies is marked by the hornblende-in isograd. The lowermost zone of the amphibolite facies is the hornblende-actinolite zone, which forms a ~3.5 km wide (N-S) zone, bounded up-grade by the oligoclase-in isograd. The plots in Fig. 5 show that variations in mineral compositions and modes are small within this zone. Hornblende comprises <20% of the total amphibole in all but one sample. Importantly, in terms of potential devolatilization, there is no decrease in the major hydrous phases, chlorite and epidote.

5.3. Lower amphibolite facies: hornblende-actinolite-oligoclase zone

The first appearance of oligoclase at the oligoclase-in isograd marks the beginning of the hornblende-actinolite-oligoclase zone, which is characterized by the assemblage Hbl + Act + Olig + Ab + Ep + Chl + Qtz + Ilm ± Ttn ± Bt ± Ms. ± Kfs ± Ap. The important modal and compositional changes, shown in Fig. 5, may be summarised as follows (all percentages within brackets refer to the average change in modal proportions within this zone calculated through subtracting the average modal proportions in the hornblende-actinolite zone from the average modes in the hornblende-actinolite-oligoclase zone): (1) the first appearance of oligoclase; (2) a decrease in the average albite content (−13%); (3) a small decrease in the total plagioclase (albite and oligoclase) content (−7%); (4) a large increase in the average hornblende content (+20%); (5) a progressive decrease in the amounts of actinolite which disappears at the top of the zone; (6) an increase in the total amphibole content (+15%); (7) a decrease in chlorite (−5% at the lower grade half of the zone; −11% in the higher grade half); (8) a small decrease in epidote (−3%); (9) the appearance of ilmenite; (10) decrease in titanite, which occurs mostly as retrograde rims around ilmenite (Fig. 5). These changes in the modal proportions reflect the following simplified reaction:

$$\text{Actinolite} + \text{Albite} + \text{Chlorite} + \text{Titanite}\ (+\text{Epidote}) = \text{Hornblende} + \text{Oligoclase} + \text{Ilmenite} + H_2O \quad (1)$$

These observations suggest that the reactions across the hornblende-actinolite-oligoclase zone account for the majority of the mineralogical transformation from a greenschist facies to amphibolite facies assemblage, and thus are the most important in terms of the

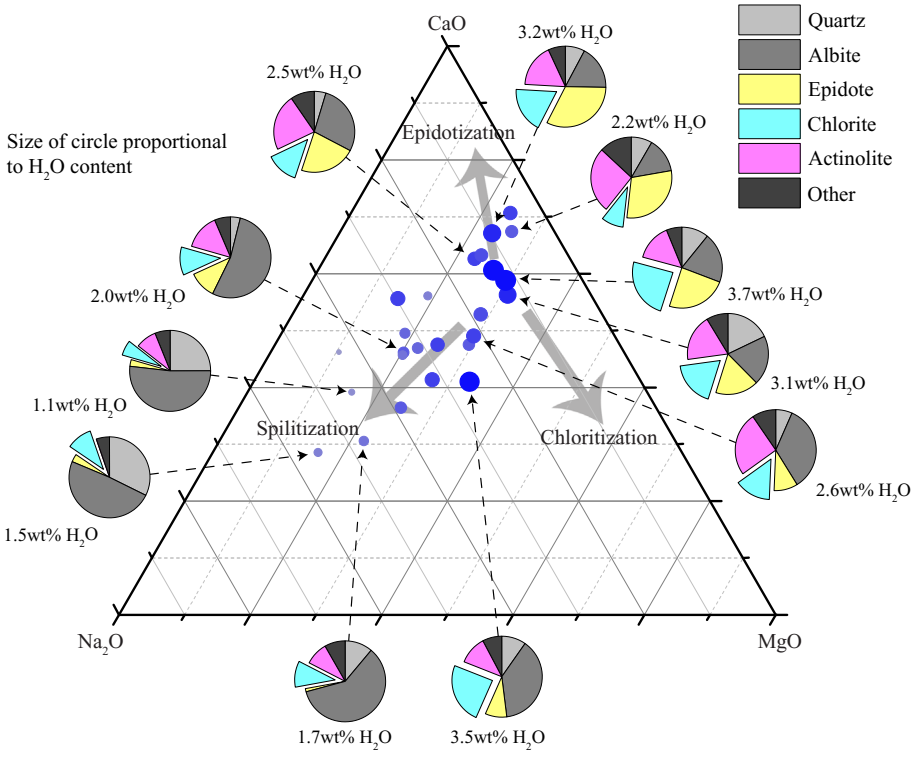

Fig. 4. H_2O contents and modal proportions within greenschist facies samples and the variation with bulk rock composition (CaO-Na_2O-MgO - wt%). Main plot shows the H_2O content (indicated by size and shade of blue circles) for samples of different bulk compositions plotted on a CaO-Na_2O-MgO compositional plot. Pie charts show the modal proportions for selected samples. The main minerals described within the 'other' category include micas, titanite, carbonate and apatite.

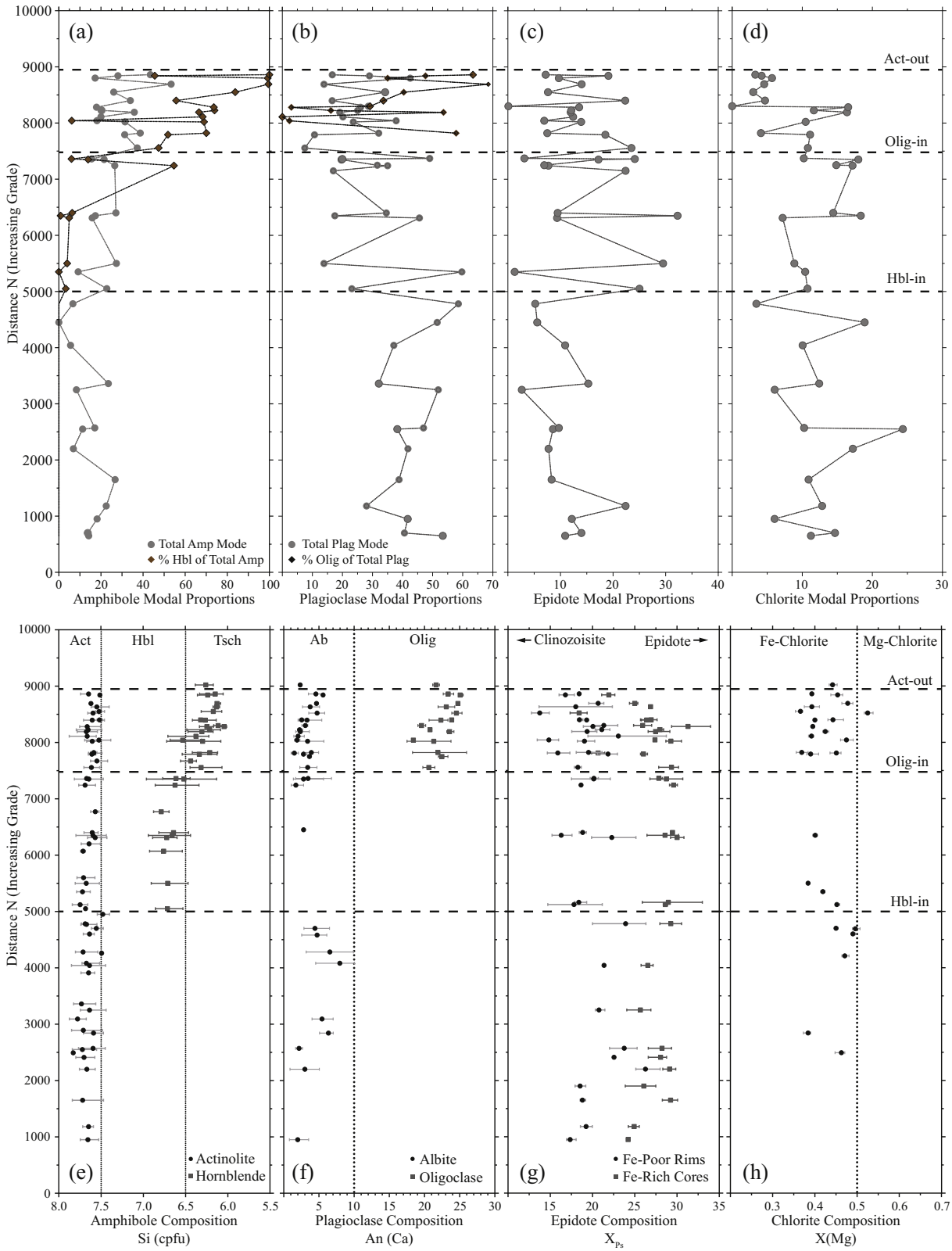

Fig. 5. Mineral modal and compositional data for the four key silicate minerals (amphibole, plagioclase, epidote and chlorite) with increasing grade. (a)-(d): Modal plots for amphibole, plagioclase, epidote and chlorite plotted versus 'distance N' (taken as a proxy for grade – see discussion in text) for samples across the greenschist and greenschist-amphibolite facies transition zones. The positions of the mineral isograds (hornblende-in, oligoclase-in and actinolite-out) are shown by the dashed lines. (e)-(h): Mineral compositions for amphibole (Si), plagioclase (An content), epidote (X_{Ps}) and chlorite (X(Mg)) plotted versus 'distance N' (increasing grade). The points represent the average composition for that sample whilst the lines represent the full range of compositions observed. Compositional fields for amphibole in Fig. 5e after Leake et al. (1997).

devolatilization across the greenschist-amphibolite facies transition. These changes account for the breakdown of ~75% of the chlorite content relative to lower grades (greenschist facies and hornblende-actinolite zone). This zone is only 1500 m wide (in a N-S direction, orthogonal to the isograds), with the majority of the chlorite breakdown occurring within the upper ~750 m.

5.4. Amphibolite facies: hornblende-oligoclase zone

The highest grade of metamorphism is observed in the northernmost portion of the field area, above which the basaltic rocks are unconformably overlain by metasediments of the Missi Group. The rocks are characterized by the absence of actinolite above the actinolite-out isograd and are predominantly composed of hornblende, plagioclase (>50% oligoclase; <50% albite), and epidote. Chlorite is a minor component, generally comprising <4% of the modal assemblage.

5.5. Carbonate and sulphide minerals

The modal amounts of carbonate and sulphide minerals relative to changing grade is shown in Fig. 6. The majority of basaltic samples contain calcite, with an average modal proportion of 1.5%, though this value is highly variable with many samples containing <1% (Fig. 6a). Dolomite was documented in only one sample, with no evidence found for ankerite or other carbonate phases. The modal proportions shown in Fig. 6a demonstrate that there are no grade-related trends in the carbonate content.

The occurrences of carbonate within the Flin Flon sequence may be explained by some or all of the following: (1) the persistence of calcite formed from pre-metamorphic hydrothermal alteration and vesicle infilling of the original basalts; (2) growth of carbonate during prograde metamorphism either due to metamorphic reactions or to fluid infiltration; (3) secondary carbonate as a result of post-metamorphic alteration.

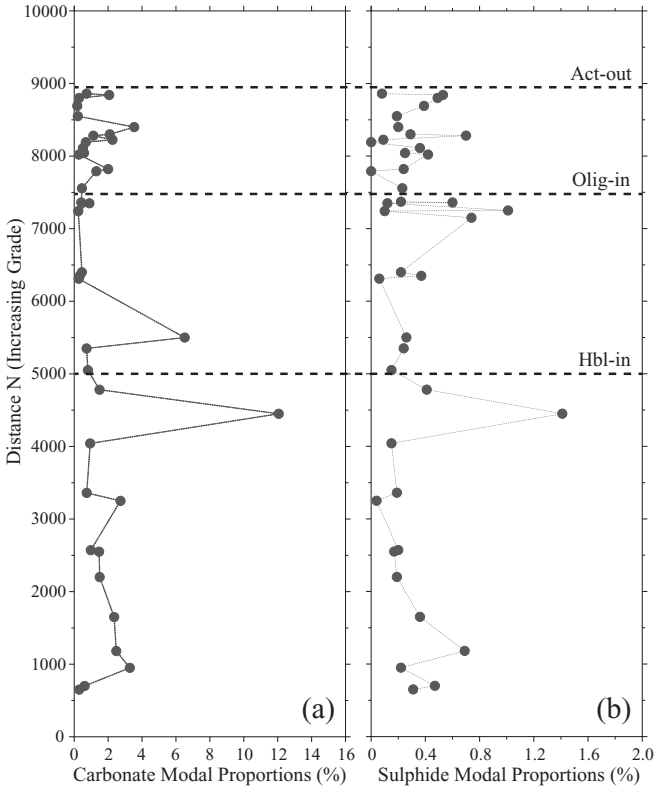

Fig. 6. Modal proportions for carbonate and sulphide group minerals versus grade (distance N) for the Flin Flon block.

The most common occurrence of carbonate is as secondary minerals, interpreted to have formed after peak metamorphism. Calcite veins and other late features such as pressure shadows around metamorphic minerals such as actinolite and hornblende (Fig. 7d) are relatively abundant features across the full range of grades. When selecting areas of the matrix for modal analysis, steps were taken to avoid obvious areas of alteration to minimize the amounts of secondary carbonates included. However, it is likely that some of the carbonate included is of post-metamorphic origin and thus the modal proportions shown in Fig. 6 likely represent maximum estimates of the carbonate present during metamorphism.

Evidence for calcite being the product of pre-metamorphic alteration is identified within the lowest grade (prehnite-pumpellyite facies) samples, where carbonate is commonly observed in relatively high modal proportions in samples that have little metamorphic overprint. Carbonate minerals are also observed as amygdules (infilled vesicles) (Fig. 7c) that likely formed during seafloor alteration. A number of pieces of evidence support the interpretation that carbonate within the prehnite-pumpellyite samples and in amygdules formed prior to regional metamorphism, including deformed carbonate-bearing amygdules which must have formed pre-deformation (and hence pre-metamorphism), and evidence for metamorphic replacement of earlier carbonate grains. This carbonation most likely occurred during seafloor alteration, but may also have occurred at some point between formation on the seafloor and deformation/metamorphism during orogenesis.

An important qualitative observation is that relatively high carbonate contents are more common in low-grade, prehnite-pumpellyite facies samples than in rocks from the greenschist and lower amphibolite facies. This is interpreted to be the result of greater preservation of pre-metamorphic carbonation within low grade samples, with the carbonate being consumed in metamorphic reactions at higher grades (greenschist and higher). Detailed quantitative modal analysis has not been carried out on the low grade samples because of their heterogeneity.

Sulphide minerals are present in very low mineral proportions (<0.5%) within most basaltic samples and occur mostly as fine grains dispersed within the matrix. The dominant sulphide minerals are chalcopyrite and pyrite, with minor sphalerite, pyrrhotite, colbaltite, and bornite. Many sulphide grains have textures that suggest a post-metamorphic origin, such as filling spaces between euhedral peak metamorphic mineralogy (e.g. amphibole needles) and cross-cutting late veins. No evidence was found for a consistent pattern of distribution of these minerals such as the disappearance or appearance of any sulphide minerals (e.g. a pyrite-out isograd), with increasing grade across the greenschist-amphibolite facies transition. However, given the sporadic and highly heterogeneous distribution of the sulphide mineralogy and difficulty in distinguishing between sulphides of pre-metamorphic or post-metamorphic origin, there remains some uncertainty in this inference.

6. Thermodynamic modelling

6.1. Phase diagram P-T modelling

Isochemical phase diagram modelling was carried out using the program Theriak-Domino, which utilizes the Gibbs free energy minimization method (de Capitani and Brown, 1987; De Capitani and Petrakakis, 2010). The internally consistent thermodynamic data set of Holland and Powell (1998; updated to version ds5.5) was utilized in conjunction with the following activity-composition (a-X) models: clino-amphibole (Diener et al., 2007, with revised mixing models from Diener and Powell, 2012), clinopyroxene (Diener and Powell, 2012; Green et al., 2007), garnet (White et al., 2007), chloritoid (White et al., 2000), chlorite (Holland et al., 1998), white mica (Coggon and Holland, 2002), biotite (White et al., 2007), epidote (Holland and Powell, 1998), spinel (White et al., 2002), ilmenite-hematite (White

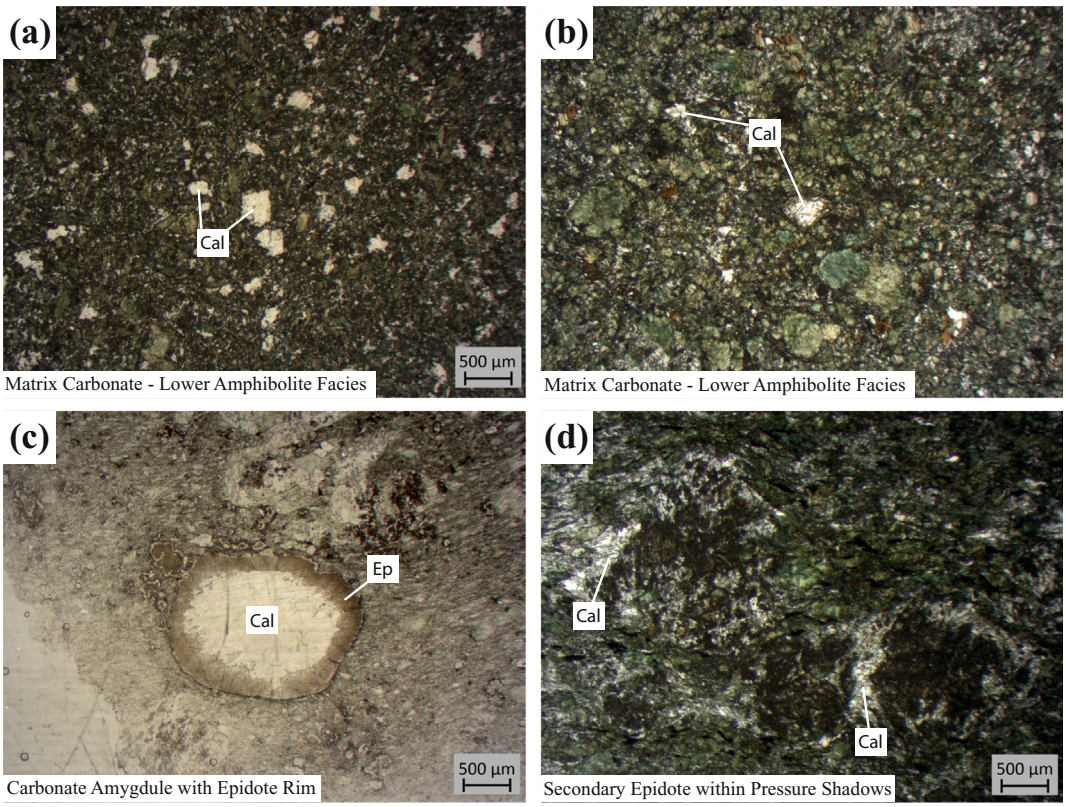

Fig. 7. Thin section photos of carbonate in greenschist and lower amphibolite facies samples. (a) Fine grained carbonate within the matrix, occurring with hornblende, actinolite, chlorite and epidote within the hornblende-actinolite-oligoclase zone; (b) Granular carbonate within a hornblende and epidote dominated matrix; (c) Large calcite amygdule rimmed by epidote; (d) Carbonate within pressure shadows around granular epidote masses.

et al., 2000; White et al., 2005) and feldspar (Holland and Powell, 2003 – Cbar-1 field model).

Pressure-temperature (P-T) modelling was carried out in the system Na_2O-CaO-K_2O-FeO-MgO-Al_2O_3-SiO_2-H_2O-TiO_2-Fe_2O_3 (NCKFMASHTO). As the ferric iron content can play a significant role in controlling the phase relations of metabasites (e.g. Diener and Powell, 2010, 2012; Rebay et al., 2010), determining an appropriate value was of crucial importance. The FeO and Fe_2O_3 contents of 8 greenschist and lower amphibolite facies samples were determined using ferrous iron titration in conjunction with XRF analysis at ACME labs in Vancouver. The determined X_{Fe3+} values (X_{Fe3+}(wt%) = Fe_2O_3/Fe_2O_3 + FeO) have an average of 26.2% with a range of 20–36%. The average X_{Fe3+} for 47 samples calculated by combining mineral modes and compositions is 18.9%, with most samples containing values between 10 and 30%. Given the potential for the XRF/titration data to be affected by oxidation during weathering and post-metamorphic alteration, the calculated X_{Fe3+} values determined from the mineral modes/compositions are interpreted to be more representative of the actual X_{Fe3+} values during metamorphism. The average calculated X_{Fe3+} values for the high-Mg bulk composition (X_{Fe3+} = 16.9%) and high-Ca bulk composition (X_{Fe3+} = 26.3%) were used for the following modelling.

Isochemical P-T phase diagrams were calculated for the average high-Mg (Fig. 8a) and high-Ca (Fig. 8b) bulk compositions. These are representative of pillow core and rim compositions respectively. Approximate pressure ranges for the Flin Flon sequence across the greenschist-amphibolite facies transition zone are shown by the grey bands in Fig. 8a and b, determined by the sequence of mineral assemblage changes, in particular the appearance of hornblende downgrade of oligoclase.

The phase diagrams in Fig. 8a and b are coloured to indicate the key assemblages across the greenschist-amphibolite facies transition zone: (1) coexisting actinolite and hornblende (coloured brown); (2) coexisting albite and oligoclase (coloured blue); (3) an 'epidote amphibolite' field characterized by coexisting epidote and hornblende (coloured yellow); and (4) a 'chlorite amphibolite' field containing coexisting chlorite and hornblende (coloured green). For the high-Mg (pillow rim) bulk composition (Fig. 8a), chlorite is predicted to be stable over a large range of P-T conditions, potentially coexisting with hornblende up to 530 °C. In contrast, the phase diagram for the high-Ca bulk composition (pillow core) (Fig. 8b) predicts a large stability field for epidote coexisting with hornblende, with epidote predicted to be stable to much higher temperatures than chlorite. Whilst the stability fields of chlorite and epidote are affected considerably by the bulk composition, the position of the hornblende-in and oligoclase-in reactions do not shift significantly.

6.2. Bulk compositional controls on hydrous mineral contents

To better characterise the bulk compositional controls on the mineral modes and bulk rock H_2O content at greenschist and amphibolite facies, a compositional space that captures as much of the compositional variation as possible was created. The CaO-Na_2O-MgO system was the starting point, as shown in Fig. 3a and b. It was found that there was systematic variation in the other important oxide components (SiO_2, FeO, Fe_2O_3, Al_2O_3) within the CaO-Na_2O-MgO compositional space. For example, SiO_2 increases towards the Na_2O corner of the diagram, FeO increases with rising MgO contents, Al_2O_3 increases slightly towards the MgO corner, whilst K_2O and TiO_2 are consistent across the diagram. Taking into account this variation, a bulk compositional space in NCKFMASHTO was created based on a CaO-Na_2O-MgO triangle within which the more minor coupled variations in the other components (SiO_2, FeO, Fe_2O_3, Al_2O_3) are linearly correlated. The corners of the triangle, labeled CaO*, Na_2O* and MgO* (Fig. 9), have the following bulk compositions:

CaO* (wt%) = SiO_2 (56.108) TiO_2 (1.020) Al_2O_3 (14.282) Fe_2O_3 (5.101) FeO (8.161) MgO (0.00) CaO (15.012) Na_2O (0.00) K_2O (0.316).
Na_2O* (wt%) = SiO_2 (70.742) TiO_2 (0.996) Al_2O_3 (12.953) Fe_2O_3 (0.00) FeO (0.00) MgO (0.00) CaO (0.00) Na_2O (15.00) K_2O (0.309).
MgO* (wt%) = SiO_2 (40.546) TiO_2 (1.014) Al_2O_3 (17.232) Fe_2O_3 (2.534) FeO (23.314) MgO (15.046) CaO (0.00) Na_2O (0.00) K_2O (0.314).

Equilibrium thermodynamic calculations were carried out for bulk compositions along a series of horizontal transects across the bulk compositional triangle in Fig. 9 using the program Theriak (de Capitani and Brown, 1987; De Capitani and Petrakakis, 2010) calculating variations in mineral modes and bulk rock H_2O content as a function of bulk composition. To compare the changes in modes across the greenschist-amphibolite facies transition zone, these diagrams were calculated at greenschist facies P-T conditions (chosen as 400 °C; 4 kbar) and amphibolite facies conditions (chosen as 4 kbar, 550 °C; equivalent of hornblende-oligoclase zone).

Figs. 9a-g show the results of the modelling for greenschist facies conditions (400 °C; 4 kbar). These diagrams show the variation in wt% H_2O contents across the bulk compositional range, as well as variations in the predicted modal proportions of amphibole (actinolite), plagioclase (albite), chlorite, epidote, titanite, and ilmenite. Amphibole modal proportions show relatively modest variation with changing bulk composition, whereas chlorite, epidote and plagioclase show large increases in modes associated with greater MgO, CaO, and Na_2O, respectively. The mineral that influences the H_2O content the most is chlorite, as revealed by the strong correlation between the location and orientation of the chlorite modal contours and the H_2O content contours. The metabasalts with compositions falling within the high-Mg group contain model H_2O contents between 3 and 4 wt%, whilst the high-Ca metabasalts are characterized by H_2O contents of 2.5–3.5 wt%. By contrast, the high-Na metabasalts contain much lower H_2O contents of 0.4-2 wt%.

The mineral modal proportions and H_2O contents are considerably different at amphibolite facies (4 kbar, 550 °C) (Figs. 9h-n). At this grade, the majority of bulk compositions from the Flin Flon sequence are predicted to no longer contain chlorite, with the exception of more Mg-rich compositions. Epidote is restricted to compositions with higher CaO contents whilst ilmenite is stable over a significant portion of the bulk compositional range. High-Mg and high-Ca bulk compositions have between 1 and 1.9 wt% H_2O whilst high-Na compositions are predicted to contain <1 wt% H_2O.

7. Modelling of fluid compositions

A number of previous studies have utilized thermodynamic modelling techniques to explore carbonate-bearing equilibria and the nature of fluids within metamorphosed mafic igneous rocks (Elmer et al., 2006; Evans et al., 2010; White et al., 2003). Elmer et al. (2006) conducted a detailed T-XCO_2 modelling study investigating the compositions of fluids derived from the greenschist-amphibolite facies transition for an average greenstone bulk composition. Our study builds upon this work by: (1) comparing modelling results with the extensive modal, mineral and bulk compositional dataset acquired for the Flin Flon sequence; and (2) illustrating how bulk compositional variation influences metamorphic assemblages, devolatilization reactions and the volume and composition of fluid released through this transition.

7.1. T-XCO_2 modelling - method

T-XCO_2 diagrams were constructed for the same average bulk compositions used in Fig. 8 for the two most common lithologies in the Flin Flon sequence: high-Mg (Fig. 10) and high-Ca (Fig. 11) metabasalts. The modelling was carried out in the NCaFMASHOC model system using a similar set of a-X models to those described previously, with the addition of the dolomite model of White et al. (2003) and a H_2O-CO_2 fluid model (Holland and Powell, 2003), and the removal of a-X models for micas and Fe—Ti oxides due to the exclusion of K_2O and TiO_2 from the chemical system. Calcite was treated as a pure end member. K and Ti

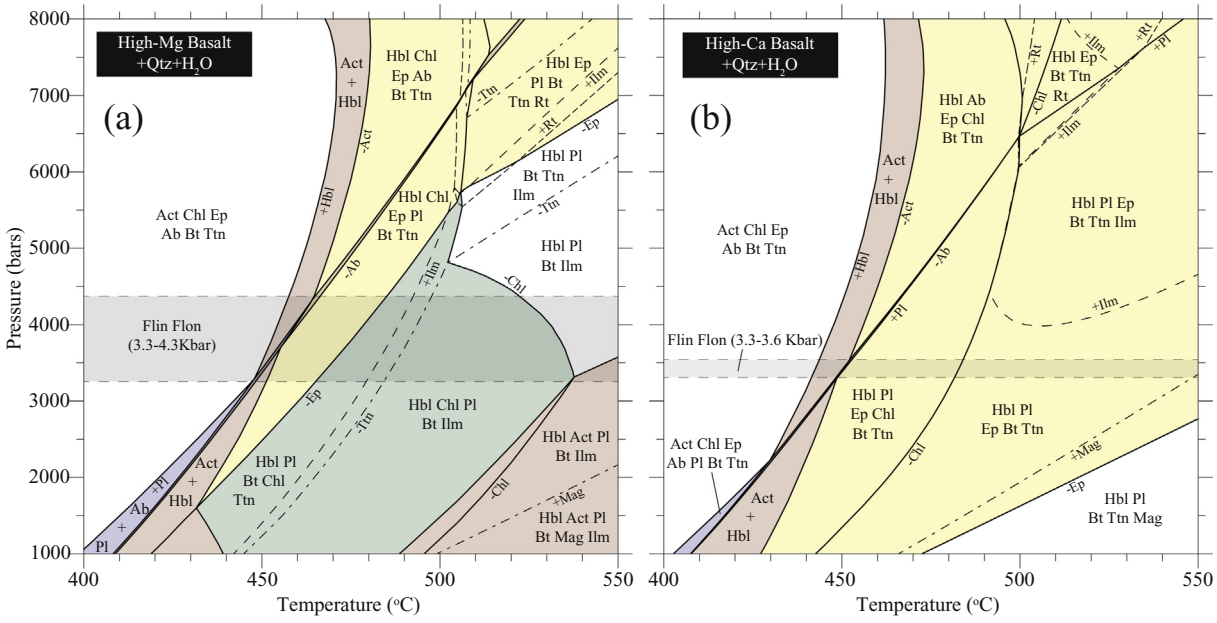

Fig. 8. Equilibrium pressure-temperature phase diagrams calculated at greenschist and amphibolite facies conditions for the: (a) average high-Mg bulk composition; and (b) average high-Ca bulk composition. Univariant lines for major minerals shown as solid lines; dashed and dotted lines used for accessory minerals (e.g. micas, Fe—Ti oxides). Fields coloured accordingly: blue = coexisting albite and oligoclase; brown = coexisting actinolite and hornblende; yellow = epidote amphibolite facies (coexisting epidote and hornblende); green = chlorite-bearing transitional assemblages (coexisting chlorite and hornblende). The grey coloured box indicates the estimated pressure range for the Flin Flon sequence based on the observed sequence of isograds (see text for discussion).

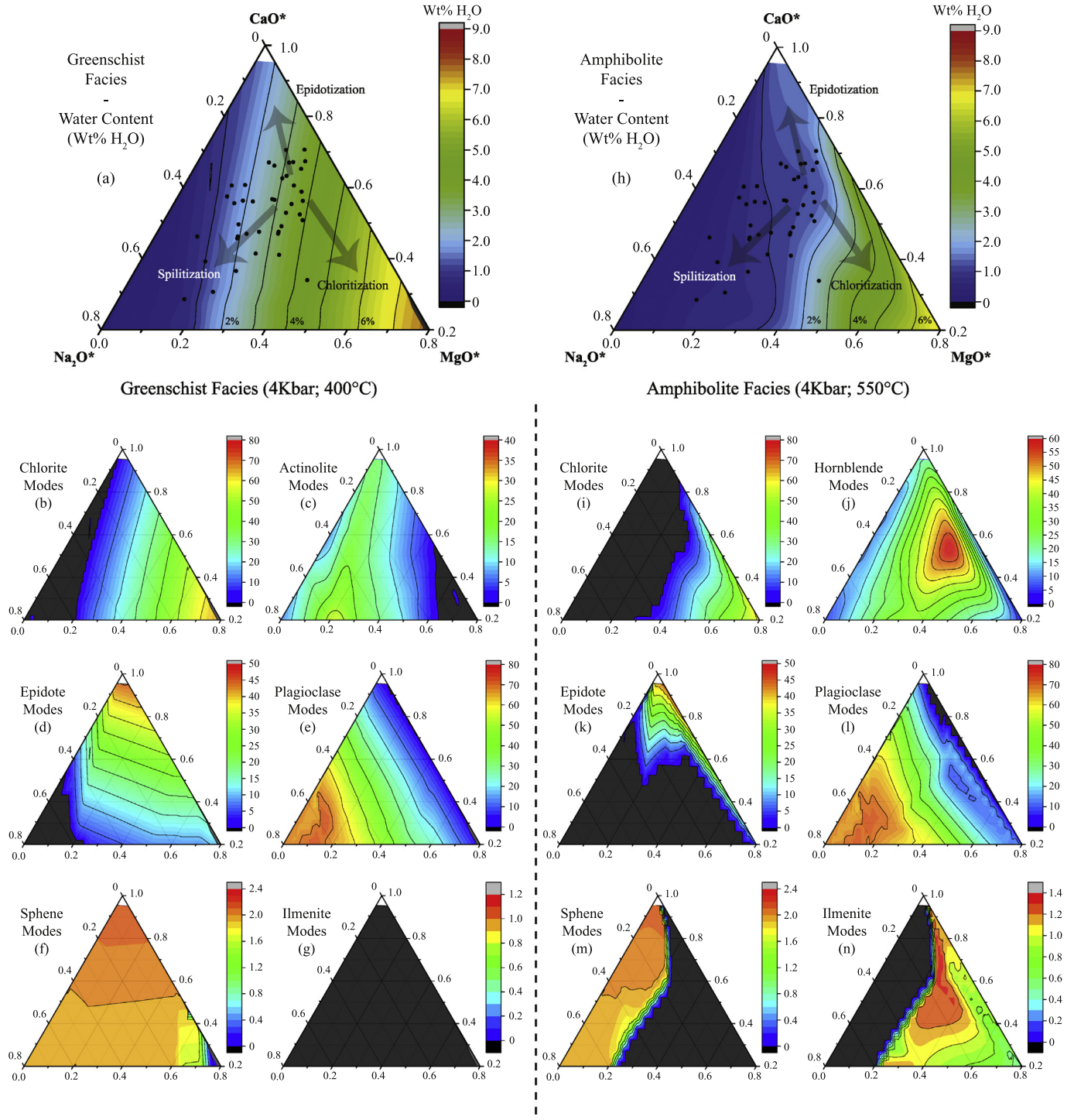

CaO* (wt%) =SiO2 (56.108) TiO2 (1.020) Al2O3 (14.282) Fe2O3 (5.101) FeO (8.161) MgO (0.00) CaO (15.012) Na2O (0.00) K2O (0.316)
Na2O* (wt%) = SiO2 (70.742) TiO2 (0.996) Al2O3 (12.953) Fe2O3 (0.00) FeO (0.00) MgO (0.00) CaO (0.00) Na2O (15.00) K2O (0.309)
MgO* (wt%) = SiO2 (40.546) TiO2 (1.014) Al2O3 (17.232) Fe2O3 (2.534) FeO (23.314) MgO (15.046) CaO (0.00) Na2O (0.00) K2O (0.314)

Fig. 9. Calculation of mineral-bound H_2O content and mineral modal proportions across a representative bulk compositional space (see definition of compositional apexes, CaO*, Na_2O* and MgO* and text description) at greenschist facies conditions (4 kbar, 400 °C) and amphibolite facies conditions (4 kbar, 550 °C). *Top diagrams:* (a) Calculated mineral-bound H_2O content (wt% values) at greenschist facies conditions (4 kbar, 400 °C); (h) Calculated mineral-bound H_2O content (wt% values) at amphibolite facies conditions (4 kbar, 550 °C). *Lower diagrams:* (b)-(g) Modal plots for the key minerals calculated at greenschist facies conditions (4 kbar, 400 °C); (i)-(n) Modal plots for the key minerals calculated at amphibolite facies conditions (4 kbar, 550 °C). The colour scale varies for different minerals depending on the range of values (see individual colour scale bars for each mineral – numbers represent the modal percentages). Note the compositional range does not include the lower 20% of the compositional range (i.e. 0–20% Ca). This is due to the lack of samples within this range and hence a lack of bulk compositional data necessary for construction of this bulk compositional space.

were excluded from the modelling as preliminary calculations found that they had little effect on the position of the main phase equilibria, and complicated the appearance of the diagram. T-XCO_2 diagrams were constructed for a pressure of 4 kbar, a temperature range of 350–600 °C, and a range of XCO_2 of 0–0.5, with fluid modelled as being in excess (Figs. 10, 11).

7.2. Predicted fluid buffering paths - method

The calculation of fluid buffering paths requires the consideration of a number of potentially unknown variables including: (1) the initial XCO_2 content of the fluid at greenschist facies conditions; (2) the amount of fluid that remains in equilibrium with the rock as the rock undergoes devolatilization along the fluid buffering path (equal to the porosity threshold); and (3) the initial carbonate content of the rock at greenschist facies conditions. The initial XCO_2 content of the fluid is unknown, though it can be partially constrained based on comparison of the T-XCO_2 diagrams (Figs. 10, 11) with the following observations from the Flin Flon sequence. The majority of greenschist facies samples contain calcite as the only carbonate phase, coexisting with actinolite, which constrains the XCO_2 content at 350 °C to very low XCO_2 contents (<0.002) such that the stable assemblage falls within a series of small fields containing coexisting calcite-actinolite. The absence of dolomite at all grades within the Flin Flon sequence suggests that the fluid buffering path should remain within the calcite-only stability field going upgrade (the spotted fields in Figs. 10, 11). Thus an initial XCO_2 value of 0.001 was used starting with the typical greenschist facies assemblage Act - Ab - Chl - Ep - Cal - Qtz.

The degree to which the fluid released from the breakdown of hydrous minerals remains within the rock has a large effect on the fluid XCO_2 evolution, and is controlled in nature by the rock porosity during metamorphism. Data regarding the porosity of greenschist and lower amphibolite facies metabasalts is limited and porosity measurements carried out on samples of greenstones may differ from the porosity during metamorphism due to a number of reasons including later deformation, post-metamorphic alteration (including surficial weathering) and the possibility of transitory porosity generated by fluid overpressure necessary for fluid escape during devolatilization (i.e. hydrofracturing). The total average porosity of a collection of greenstone samples was estimated to be 0.669% by Norton and Knapp (1977) which, given the aforementioned limitations, likely represents only an approximate estimate of the porosity during metamorphism. Based on the above considerations, a porosity of 0.5% was used for initial modelling. A variety of higher and lower porosities were tested to examine the consequences of varying porosity on the XCO_2 buffering paths (see supplementary information, Fig. S1). In general, paths calculated with lower porosities show greater shifts to higher XCO_2 during decarbonation and lower XCO_2 during dehydration (Fig. S1).

Fluid buffering paths were calculated for the high-Mg (Fig. 10) and high-Ca (Fig. 11) bulk compositions using initial carbonate contents representing the observed average, minimum (zero) and maximum carbonate modal contents for each compositional group. The fluid buffer paths represent the predicted changing XCO_2 content of the fluid with increasing temperature and changing mineral assemblage.

7.3. Predicted T-XCO_2 modelling and fluid buffering paths for the Flin Flon Volcanics

Fig. 10a shows the T-XCO_2 diagram and three fluid buffer paths calculated using the average, minimum (zero) and maximum carbonate contents for the high-Mg samples. Fig. 10b-d shows the predicted variation in the modal proportions of the main phases and the amount of fluid released (in moles) with increasing temperature along each of these buffer paths, which can be used in conjunction with the XCO_2 fluid buffer paths to assess the combined amounts and compositions of fluid released.

For the high-Mg composition, the total fluid predicted to be released across the greenschist-amphibolite facies transition is ~5.9–9.3 mol, depending upon the initial carbonate content. This devolatilization results predominantly from the breakdown of chlorite, and is predicted to occur in five discrete intervals of fluid release for a sample with an average carbonate content. The first is associated with entry into the coexisting actinolite and hornblende field at 450 °C (point 1 in Fig. 10), in which there is a marked predicted increase in the amount of hornblende and reduction in the amount of chlorite, actinolite, epidote and albite. This results in the predicted release of approximately 1.5 mol of fluid (~24% of total fluid), with a low XCO_2 of ~0.025. The second major predicted interval of fluid release (point 2 in Fig. 10) occurs over the span of only ~2 °C, immediately up-grade of an oligoclase-producing reaction at 458 °C. This reaction involves the formation of oligoclase and more hornblende, the complete consumption of albite, and a modal reduction in chlorite and epidote, resulting in the release of 1.7 mol of fluid (~27% total) with an XCO_2 of 0.028. The third predicted interval of fluid release (point 3) is associated with the final consumption of epidote, across a temperature window of ~10 °C, resulting in 1.1 mol of fluid accounting for ~17% of the total fluid release, with an XCO_2 of 0.028–0.050. The fourth interval is associated with the complete consumption of carbonate (calcite) over a ~5 °C interval in the upper part of the Cal-Hbl-Chl-Pl field, with the release of 0.6 mol of fluid (10% total fluid loss). The XCO_2 of the fluid released going through this interval is predicted to change from 0.12 to 0.23 because the fluid composition is buffered to higher XCO_2 contents within the Cal-Hbl-Chl-Pl field as a result of the continuous breakdown of calcite. The last predicted interval of fluid release results from the final breakdown of the remaining chlorite (~540–550 °C) within the Hbl-Chl-Pl field, causing the loss of approximately 0.7 mol of fluid (11% total fluid loss) with an XCO_2 content of 0.08.

For the high-Mg basalt, the fluid buffering path for the maximum carbonate content (4.2%) (Fig. 10c) is predicted to follow a broadly similar evolution to that for the average carbonate buffering path. However, a number of important differences occur: (1) there is a much larger fluid loss within the Cal-Hbl-Chl-Pl field (point 4; Fig. 10); (2) fluids are generally buffered to higher XCO_2 contents, particularly within the Cal-Hbl-Chl-Pl field (point 4) where fluids released over this interval have predicted XCO_2 contents of 0.22 to 0.42. The predicted reactions and resulting devolatilization intervals for the carbonate-absent system (Fig. 10d) are similar to those of the average carbonate system (Fig. 10b), in terms of the amounts of fluid loss and temperature intervals. However, in contrast to the carbonate-present systems, there is no fluid loss reaction equivalent to point 4 (Fig. 10d), suggesting that the loss of chlorite and resulting devolatilization over this interval is only driven by the presence and subsequent loss of carbonate.

The T-XCO_2 diagram for the high-Ca basalt (Fig. 11a) shows three major differences from that of the high-Mg basalt: (1) a larger predicted stability field for epidote-bearing assemblages (shown in yellow); (2) a reduced stability field for chlorite; and (3) an increase in the stability of calcite to higher temperatures (shown by the dotted field in Fig. 11). Buffering paths were calculated for average (1.72%) and maximum (5.91%) carbonate contents, which are slightly higher carbonate proportions than for the high-Mg basalts. The fluid buffering paths follow a similar trajectory to those for the high-Mg basaltic composition, passing through the coexisting actinolite-hornblende field (point 1 in Fig. 11) and then the narrow temperature interval within which oligoclase appears and albite is consumed (point 2). A large amount of fluid loss (2.6 mol; 37% total fluid loss for the average carbonate path) is predicted to occur concomitant with the breakdown of chlorite, epidote, and carbonate to form hornblende within the Cal-Hbl-Chl-Ep-Pl field (point 3). These paths differ from those for the high-Mg basalt, with fluid buffering paths for the high-Ca composition losing chlorite before calcite, and epidote persisting up to higher temperatures. This difference is important because, whilst the equilibrium fluid compositions is buffered to higher XCO_2 contents within the Cal-Hbl-Ep-Pl field as a function of the greater carbonate contents, the volume of fluid released with this composition is minimal because chlorite has already been consumed. Thus, for the average carbonate system, only a small volume of fluid is predicted to be released with XCO_2 compositions exceeding 0.125, despite the fluid compositions in equilibrium with the rock being buffered to much higher XCO_2 contents.

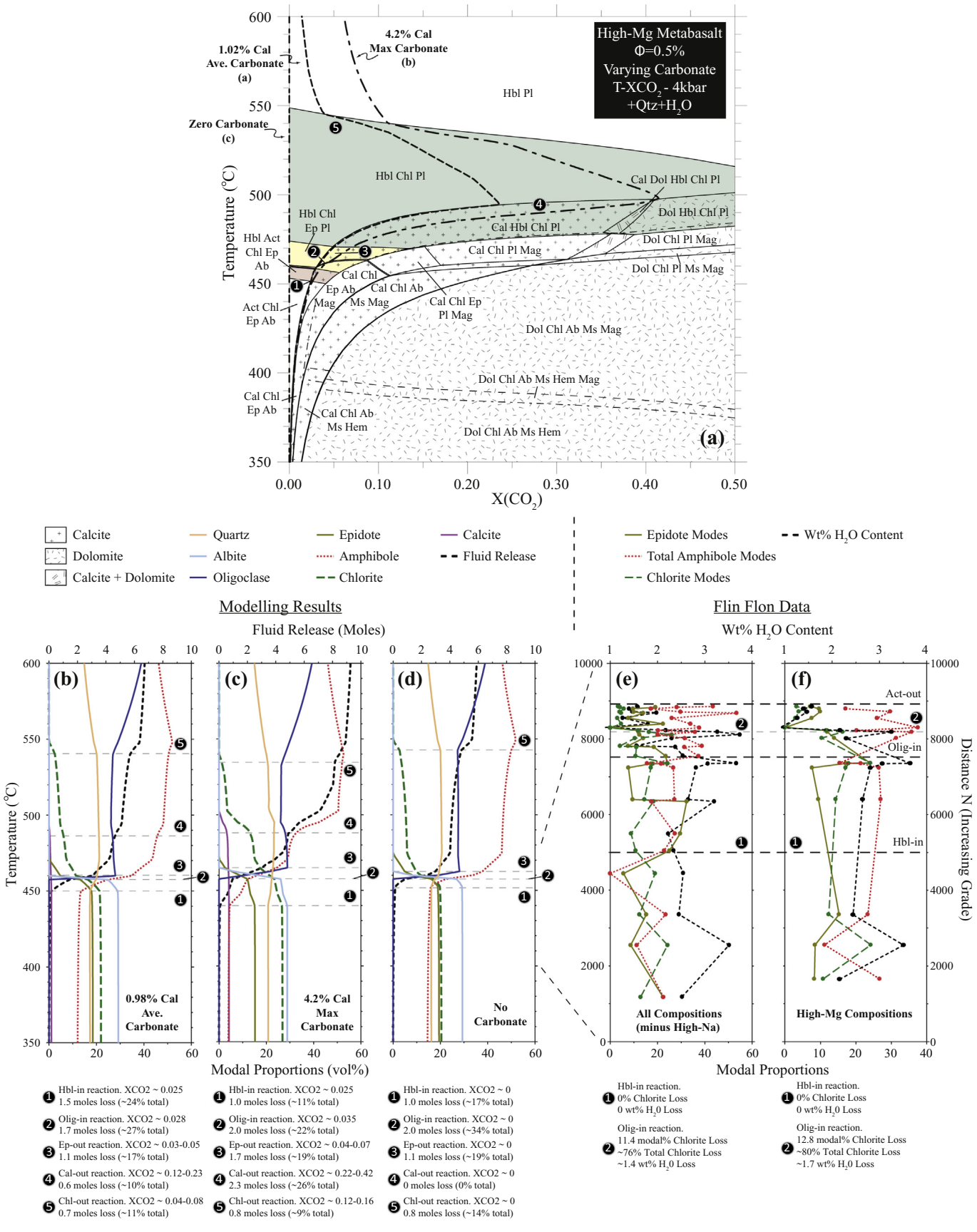
High-Mg Metabasalt
Φ=0.5%
Varying Carbonate
T-XCO2 - 4kbar
+Qtz+H2O
1.02% Cal
Ave. Carbonate
(a)
4.2% Cal
Max Carbonate
(b)
Zero Carbonate
(c)
Hbl Pl
Hbl Chl Pl
Cal Dol Hbl Chl Pl
Dol Hbl Chl Pl
Hbl Chl
Ep Pl
Cal Hbl Chl Pl
Hbl Act
Chl Ep
Ab
Cal Chl Pl Mag
Dol Chl Pl Mag
Dol Chl Pl Ms Mag
Cal Chl
Ep Ab
Mag
Cal Chl Ab
Ms Mag
Cal Chl Ep
Pl Mag
Act Chl
Ep Ab
Dol Chl Ab Ms Mag
Dol Chl Ab Ms Hem Mag
Cal Chl
Ep Ab
Cal Chl Ab
Ms Hem
Dol Chl Ab Ms Hem
(a)
Temperature (°C)
X(CO2)
Calcite
Dolomite
Calcite + Dolomite
Quartz
Albite
Oligoclase
Epidote
Amphibole
Chlorite
Calcite
Fluid Release
Epidote Modes
Total Amphibole Modes
Chlorite Modes
Wt% H2O Content
Modelling Results
Flin Flon Data
Fluid Release (Moles)
Wt% H2O Content
(b)
(c)
(d)
(e)
(f)
0.98% Cal
Ave.
Carbonate
4.2% Cal
Max
Carbonate
No
Carbonate
All Compositions
(minus High-Na)
High-Mg Compositions
Act-out
Olig-in
Hbl-in
Distance N (Increasing Grade)
Modal Proportions (vol%)
Modal Proportions
1 Hbl-in reaction. XCO2 ~ 0.025
1.5 moles loss (~24% total)
2 Olig-in reaction. XCO2 ~ 0.028
1.7 moles loss (~27% total)
3 Ep-out reaction. XCO2 ~ 0.03-0.05
1.1 moles loss (~17% total)
4 Cal-out reaction. XCO2 ~ 0.12-0.23
0.6 moles loss (~10% total)
5 Chl-out reaction. XCO2 ~ 0.04-0.08
0.7 moles loss (~11% total)
1 Hbl-in reaction. XCO2 ~ 0.025
1.0 moles loss (~11% total)
2 Olig-in reaction. XCO2 ~ 0.035
2.0 moles loss (~22% total)
3 Ep-out reaction. XCO2 ~ 0.04-0.07
1.7 moles loss (~19% total)
4 Cal-out reaction. XCO2 ~ 0.22-0.42
2.3 moles loss (~26% total)
5 Chl-out reaction. XCO2 ~ 0.12-0.16
0.8 moles loss (~9% total)
1 Hbl-in reaction. XCO2 ~ 0
1.0 moles loss (~17% total)
2 Olig-in reaction. XCO2 ~ 0
2.0 moles loss (~34% total)
3 Ep-out reaction. XCO2 ~ 0
1.1 moles loss (~19% total)
4 Cal-out reaction. XCO2 ~ 0
0 moles loss (0% total)
5 Chl-out reaction. XCO2 ~ 0
0.8 moles loss (~14% total)
1 Hbl-in reaction.
0% Chlorite Loss
0 wt% H2O Loss
2 Olig-in reaction.
11.4 modal% Chlorite Loss
~76% Total Chlorite Loss
~1.4 wt% H2O Loss
1 Hbl-in reaction.
0% Chlorite Loss
0 wt% H2O Loss
2 Olig-in reaction.
12.8 modal% Chlorite Loss
~80% Total Chlorite Loss
~1.7 wt% H2O Loss

8. Discussion – metamorphic devolatilization across the greenschist-amphibolite facies transition

In the following sections, natural observations from the Flin Flon sequence are compared to, and integrated with, the predictions derived from the thermodynamic modelling. This provide insights into the devolatilization reaction intervals, and the amounts and compositions of fluids produced across the greenschist-amphibolite facies transition zone in metabasites. This information is used to evaluate these fluids as being the possible source fluids for orogenic gold deposit formation.

8.1. Fluid sources for orogenic gold deposition

There exists much debate as to the source of fluids that produce orogenic gold deposits (e.g. Elmer et al., 2006; Gaboury, 2013; Goldfarb et al., 2005; Goldfarb and Groves, 2015; Groves et al., 1998; Phillips and Powell, 2009, 2010; Powell et al., 1991; Tomkins, 2010, 2013; Xue et al., 2013). The different suggested fluid sources can be broadly separated into two main categories: (1)fluids released during the crystallization of felsic-intermediate magmas (e.g. Xue et al., 2013); and (2) metamorphic fluids, most commonly interpreted to result from the breakdown of hydrous minerals across the greenschist-amphibolite facies transition zone (e.g. Elmer et al., 2006; Phillips and Powell, 2010; Powell et al., 1991; Tomkins, 2010, 2013). The majority of recent work has favoured a metamorphic origin (e.g. Goldfarb and Groves, 2015; Phillips and Powell, 2010; Tomkins, 2010, 2013) for a number of reasons including better consistency with geological and geochemical features, such as fluid inclusion and stable isotope data, and a stronger chronological link between metamorphism and orogenic gold formation (e.g. Goldfarb and Groves, 2015). Some studies have argued that metamorphosed carbonated mafic rocks are the most likely source rocks for these gold bearing fluids (e.g. Elmer et al., 2006; Phillips and Powell, 2010; Powell et al., 1991), whilst others have suggested metamorphosed carbonaceous sedimentary rocks may provide a more likely source (e.g. Gaboury, 2013; Large et al., 2011; Tomkins, 2010, 2013).

Whether the source rock is metavolcanic or metasedimentary, the metamorphic devolatilization model (e.g. Phillips and Powell, 2010) suggests that Au-bearing fluids are produced across the greenschist-amphibolite facies transition zone, migrate from the host rocks, and cause gold deposition and the formation of large fluid alteration haloes at higher levels of the crust. Ideal metamorphic devolatilization source areas are suggested to have the ability to: (1) produce significant volumes of fluid; (2) release gold, likely in the form of hydrosulphide complexes (e.g. $Au(HS)_2^-$ and AuHS); and (3) to produce fluids with moderate XCO_2 compositions (e.g. Phillips and Powell, 2010; Tomkins, 2010, 2013).

The source of both the gold and the associated sulphur within the metamorphic devolatilization model is suggested to be the breakdown of pyrite to pyrrhotite, which liberates sulphur ($FeS_2 = FeS + 1/2S_2$) (e.g. Phillips and Powell, 2010; Pitcairn et al., 2006, 2010, 2015; Tomkins, 2010). Trace element analyses of phases within greenschist and amphibolite facies samples suggest that pyrite is the main carrier of gold within rocks of this grade (e.g. Pitcairn et al., 2006). A number of field based studies have documented changes in sulphide mineralogy during prograde metamorphism, though this work has been focused on meta-sedimentary sequences (e.g. Ferry, 1981; Pitcairn et al., 2006, 2010, 2015).

Fluids associated with orogenic gold deposits have been interpreted as being mixed H_2O-CO_2 fluids with fairly consistent moderate XCO_2 (e.g. 0.2–0.3) compositions based on fluid inclusion data and on the presence of carbonate phases within gold-bearing veins (e.g. Gaboury, 2013; Groves et al., 1998; Kerrich and Fyfe, 1981; Ridley and Diamond, 2000). In addition, it has also been suggested that CO_2 plays an important chemical role in gold transport by buffering the pH of fluids such that higher concentrations of gold hydrosulphide complexes can be maintained (Phillips and Evans, 2004). Thus, in order for a metamorphic devolatilization source fluid to be consistent with these observations, it should have moderate XCO_2 values (~0.2–0.3) (Elmer et al., 2006; Phillips and Powell, 2010). A detailed T-XCO_2 modelling study of greenschist-amphibolite facies rocks by Elmer et al. (2006), utilizing similar modelling methods used in this paper, suggested that moderate XCO_2 values (0.2–0.3) may be produced by the coincident breakdown of carbonate and chlorite within carbonate-rich mafic rocks.

This study builds upon this previous work by adding constraints and insights from an exceptionally well characterized natural sequence utilizing: (1) a uniquely detailed documentation of modes, compositions and textures of hydrous mineralogy as well as carbonate and sulphide minerals; (2) field documentation of the dehydration reaction progress and assessment of the relative important of different reactions involved; (3) a large bulk compositional database and documentation of pre-metamorphic alteration processes.

8.2. Comparison of predicted versus observed amounts of fluid release across the greenschist-amphibolite facies transition

Table 1 summarizes the petrological and modelling estimates for bulk rock mineral-bound H_2O contents (wt%) from greenschist and amphibolite facies samples, as well as the average dehydration amounts (wt%) for each bulk composition type calculated by subtracting the average greenschist and amphibolite H_2O contents. The bulk rock H_2O contents (wt%) of Hacker et al. (2003) are also included for comparison, which were estimated from a compilation of modal data for greenschist and amphibolite facies metabasalts that approximate MORB bulk compositions (see Hacker et al., 2003 for a full description of the method).

A comparison of the modelling and petrological estimates of the mineral-bound whole-rock H_2O contents in Table 1 suggests that the modelling slightly over-estimates the amount of devolatilization compared to the modal estimates (by ~0.4–0.7 wt%; Table 1). The estimated H_2O contents for greenschist facies assemblages vary depending on the bulk composition, with the high-Mg compositions having the highest H_2O contents (petrological estimate: 3.1 wt%; modelling estimate: 3.5 wt%), the high-Ca compositions having slightly lower H_2O contents (petrological estimate: 2.8 wt%; modelling estimate: 3.1 wt%), and the high-Na basalts having the lowest H_2O contents (petrological estimate: 1.7 wt%; modelling estimate: 1.6 wt%) (Table 1). The calculated mineral-bound H_2O contents at amphibolite facies conditions vary less across the range of bulk rock compositions, with an average of 1.3 wt%

Fig. 10. T-XCO_2 and fluid buffer path modelling for the average high-Mg basaltic composition (fixed porosity, varying carbonate contents) and comparison with modal data from the Flin Flon sequence. (a) T-XCO_2 diagram calculated for the average high-Mg basalt. The transitional fields are coloured using the same scheme previously described for Fig. 8 and in the text. In addition, carbonate-bearing fields contain patterns indicating the type of carbonate present (calcite, dolomite or both). The major phases of fluid release that occur are labeled on both the phase diagram and in the modal plots (see text for discussion). (b)-(d) Fluid buffering paths calculated using a 0.5% porosity model (see text for description) for different starting carbonate contents: (b) average carbonate (0.98%); (c) maximum carbonate (4.2%); (d) carbonate-free system. The solid coloured lines represent the modal proportions (%) for the major phases (see bottom scale) whilst the thick dashed black lines represent the fluid release in moles (see top scale). The numbers correspond to the key intervals of devolatilization as described in the text. The reactions are listed below the diagram with the approximate compositions and amounts of the fluid released associated with each interval. (e) Modal plot for samples from all bulk compositional groups (excluding high-Na bulk compositions) for the key hydrous phases amphibole, epidote and chlorite plotted versus 'distance N' (taken as a proxy for grade – see discussion in text) for samples across the greenschist and greenschist-amphibolite facies transition zones (see bottom scale). In addition, the calculated hydrous content of the rock is shown by the dashed black line (see top scale). (f) Modal plot for high-Mg basaltic samples for the key hydrous phases amphibole, epidote and chlorite (see bottom scale) plus the calculated hydrous content (see top scale) plotted versus 'distance N'.

for high-Mg compositions (modelling estimate: 1.3 wt%) and 1.7 wt% for high-Ca compositions (modelling estimate: 1.3 wt%). It was not possible to estimate an average observed H_2O content for the high-Na bulk composition at amphibolite facies conditions due to the lack of samples at this grade and bulk composition at Flin Flon.

Comparison of the average H_2O contents at greenschist and amphibolite facies is used to estimate the metamorphic devolatilization occurring across the greenschist-amphibolite facies transition (Table 1). High-Mg and high-Ca basalts, representative of pillow rim and core material, undergo an average H_2O loss of 1.8 wt% (modelling estimate: 2.2 wt%) and 1.1 wt% (modelling estimate: 1.8 wt%), respectively. Whilst it was not possible to estimate the average H_2O loss for high-Na basalts using the Flin Flon suite, due to the lack of samples at amphibolite facies conditions, the thermodynamic modelling predicts that they will generate smaller volumes of fluids, ranging from <0.1 wt% to 1.1 wt% (average: 0.9 wt%), which is consistent with the lower observed H_2O contents within greenschist facies samples of this bulk composition. These results show that the amount of devolatilization is strongly controlled by the bulk composition, which is interpreted to mainly reflect pre-metamorphic alteration processes.

8.3. Comparison of predicted versus observed devolatilization intervals across the greenschist-amphibolite facies transition zone

In order to compare the predicted versus model devolatilization intervals, the observed modal abundances and bulk rock wt% H_2O contents from the Flin Flon sequence are plotted in Figs. 10 and 11 (Fig. 10e, f; Fig. 11e, f) alongside the modal evolution and fluid release predicted by the modelling for different carbonate contents (Fig. 10b, c, d; Fig. 11b, c, d). The observed modal abundances and bulk rock H_2O contents are shown in two plots in Figs. 10 and 11, with the first (Figs. 10e, 11e) showing the modal abundances of the main hydrous minerals (chlorite, epidote and amphibole) for samples from all bulk compositional groups (excluding high-Na compositions, which have highly variable modal abundances) and the second (Figs. 10f, 11f) showing the modal changes for the selected relevant bulk compositional group (i.e. high-Mg basalts in Fig. 10f; high-Ca basalts in Fig. 11f). For practical calculation reasons, the thermodynamically predicted fluid release is given in moles of fluid lost from the system, whilst the observed fluid release is described in terms of changes in bulk rock H_2O content. As discussed in Section 8.2, the total amounts of devolatilization across the transition zone are broadly similar comparing the modelling predictions with the estimated observed fluid release (Table 1).

In the following section, the relative importance of different devolatilization intervals are discussed utilizing the Flin Flon observations and modelling predictions. For ease of comparison in this discussion and in Figs. 10 and 11, the fluid release is largely considered in terms of proportions of the total fluid loss and in terms of the modal abundance of chlorite, the breakdown of which accounts for the vast majority of fluid loss.

Within the hornblende-actinolite zone in the Flin Flon sequence, mineralogical change is limited with no consistent change in the proportions of chlorite and other hydrous mineralogy (e.g. epidote) (Fig. 5; Fig. 10e, f; Fig. 11e, f). Thermodynamic modelling for both high-Mg and high-Ca bulk compositions (Figs. 10, 11), suggests a similar predicted reaction interval (point 1 in Figs. 10, 11) marking the first appearance of hornblende, coexisting with actinolite, albite, chlorite and epidote. However, in contrast to the observations from Flin Flon, the modelling predicts significant changes across the interval (the brown field in Figs. 10 and 11) including: the complete replacement of actinolite by hornblende; a significant increase in the total amphibole content (from 13% to 25% for the average carbonate buffering path for the high-Mg bulk composition; Fig. 10b); and notable decreases in the proportions of the hydrous minerals chlorite (from 22% to 15%; Fig. 10b) and epidote (from 18% to 13%; Fig. 10b). The observed modal proportions of hydrous minerals within the hornblende-actinolite zone at Flin Flon suggests that the devolatilization within the hornblende-actinolite zone is very minor, comprising a minimal proportion of the total fluid loss and no chlorite loss (Fig. 10e, f; Figs. 11e, f). By contrast, the thermodynamic modelling suggests a much higher amount of fluid loss for the high-Mg compositions associated with ~5 modal% chlorite breakdown (~24% total fluid loss; average carbonate buffering path; point 1 in Fig. 10b).

Significant changes in the observed modal mineralogy occur within the hornblende-actinolite-oligoclase zone in the Flin Flon sequence (Fig. 5; Fig. 10e, f; Figs. 11e, f). The modal proportions of the hydrous minerals drop significantly, with chlorite decreasing by ~11 modal% on average from ~15% average in the greenschist facies to 4% in the highest grade part of the hornblende-actinolite-oligoclase zone (~13 modal% average decrease for high-Mg basalts; ~8 modal% average decrease for high-Ca basalts) (Fig. 10e, f; Fig. 11e, f). The thermodynamic modelling also predicts a significant interval of devolatilization accompanying the first appearance of oligoclase (point 2; Figs. 10, 11), which coexists with albite over a very small temperature interval (~2 °C) and is associated with an increase in predicted hornblende modes from 26% to 34% (high-Mg composition, average carbonate content) (Fig. 10b). However, in contrast to observations from Flin Flon, albite completely disappears over this small temperature interval and the decrease in the main hydrous mineral, chlorite, is relatively minor (15% to 11%) (Fig. 10b). The modelling predicts a significant decrease in the epidote content (13% to 5%) which is not observed in the Flin Flon sequence (Fig. 10b).

The estimated observed H_2O release across the hornblende-actinolite-oligoclase zone at Flin Flon is approximately 1-2 wt%, depending on bulk composition, driven by the breakdown of ~75% of the total chlorite content (average 11 modal% loss) (Table 1; Fig. 10e, f; Figs. 11e, f). The predicted H_2O release from thermodynamic modelling over the approximately equivalent interval marking the appearance of oligoclase is considerably less than the observed fluid release, accounting for only 27% of the total fluid loss and ~4 modal% chlorite breakdown for the high-Mg bulk compositions (average carbonate content) (Fig. 10b).

The thermodynamic modelling suggests continued devolatilization at grades above those of the main greenschist-amphibolite facies transition zone (Figs. 10, 11). These reactions are predicted to happen at considerably higher temperatures than the first appearance of oligoclase and thus they would likely occur at higher grades than those observed within the Flin Flon sequence. This fluid release results from the predicted persistence of chlorite and epidote to higher grades where they are predicted to break down to form more hornblende over a number of devolatilization intervals (points 3, 4 and 5 in Fig. 10; points 3 and 4 in Fig. 11). For the high-Mg bulk composition, epidote is predicted to disappear shortly after the appearance of oligoclase (point 3; Fig. 10) whilst chlorite survives ~90 °C past the first appearance of hornblende, reacting out over two intervals (points 4 and 5; Fig. 10). By contrast, for the high-Ca bulk rock composition, chlorite is predicted to disappear at grades just above the appearance of oligoclase (point 3; Fig. 11), whilst epidote persists to much higher grade, breaking down continuously over a ~100 °C interval (point 4; Fig. 11).

Whilst the final breakdown of chlorite and epidote are not seen in the Flin Flon rocks, the observations from this sequence are useful in interpreting potential further devolatilization at higher metamorphic grades. As discussed above, the majority of the chlorite (~75%) is consumed across the hornblende-actinolite-oligoclase zone and the low proportions of chlorite in the upper part of the hornblende-actinolite-oligoclase zone (average mode: 4%) suggests that devolatilization at higher grades would be limited. Thus the significant thermodynamically predicted devolatilization intervals at higher grades for the high-Mg bulk composition (points 4 and 5; Fig. 10) seem unlikely to occur at higher grades in the Flin Flon sequence. By contrast, epidote shows no decrease in modal proportions across the transition, interpreted as

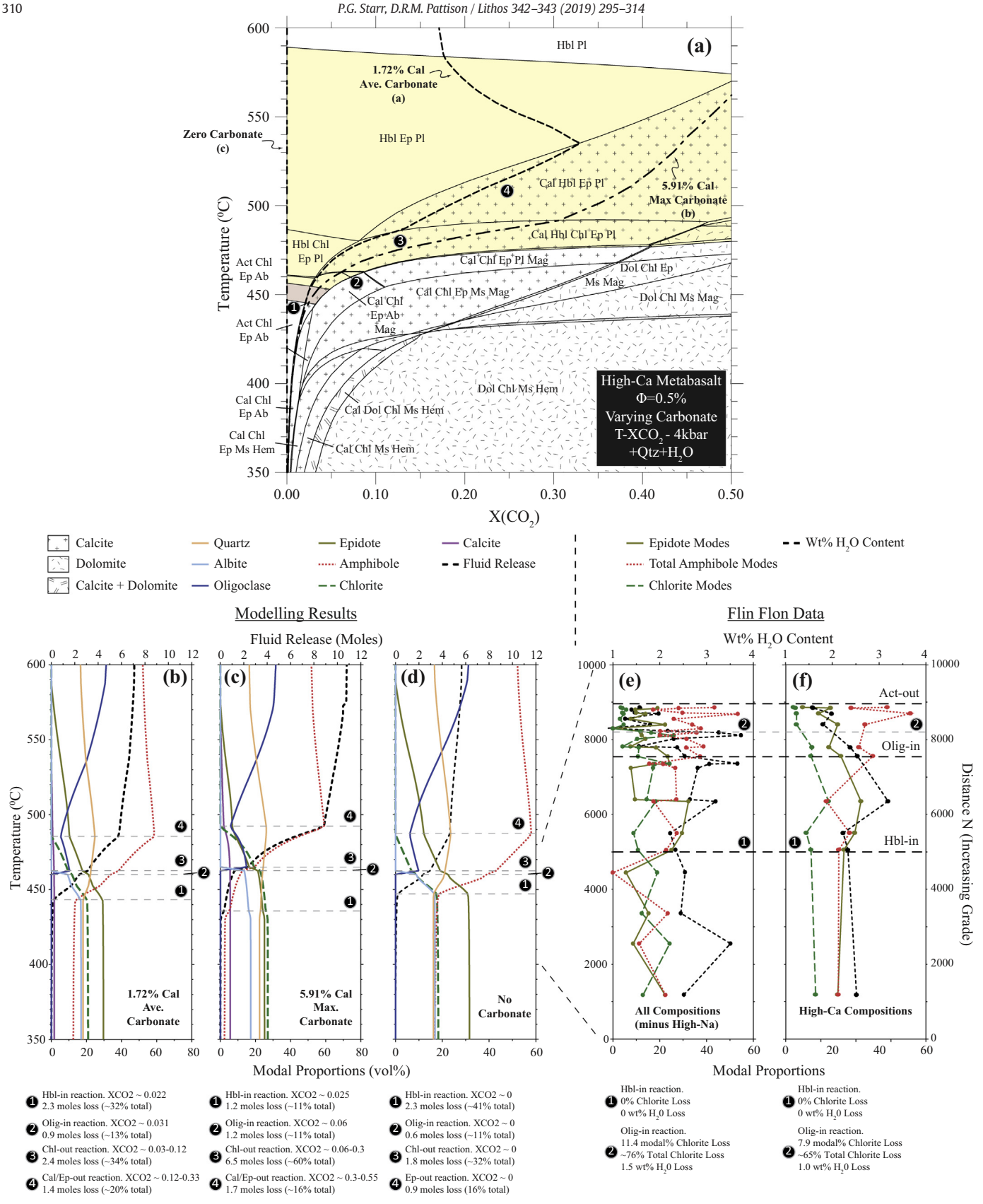

Fig. 11. T-XCO_2 and fluid buffer path modelling for the average high-Ca basaltic composition (fixed porosity, varying carbonate contents). (a) T-XCO_2 diagram calculated for the average high-Ca basalt. (b)-(d) Fluid buffering paths are calculated using a 0.5% porosity model (see text for description) for different starting carbonate contents: (b) average carbonate (1.72%); (c) maximum carbonate (5.91%); (d) carbonate-free system. The solid coloured lines represent the modal proportions (%) for the major phases (see bottom scale) whilst the thick dashed black lines represent the fluid release in moles (see top scale). (e) Modal plot for samples from all bulk compositional groups (excluding high-Na bulk compositions) for the key hydrous phases amphibole, epidote and chlorite plotted versus 'distance N' for samples across the greenschist and greenschist-amphibolite facies transition zones (see bottom scale). In addition, the calculated hydrous content of the rock is shown by the dashed black line (see top scale). (f) Modal plot for high-Ca basaltic samples for the key hydrous phases amphibole, epidote and chlorite (see bottom scale) plus the calculated hydrous content (see top scale) plotted versus 'distance N'.

reflecting the sluggish dissolution kinetics of epidote leading to its persistence to higher grade as a metastable relic (Starr and Pattison, 2019). The breakdown of this epidote must occur at some point, resulting in a smaller devolatilization event at higher grades, though it is unclear whether this devolatilization would occur as a pulse over a small, kinetically-overstepped, temperature interval or as a more gradual or sequential event.

In summary, comparison of the observations from Flin Flon with the modelled phase equilibria suggests a broadly comparable sequence of mineral assemblage changes, including the sequential appearance of hornblende, followed by oligoclase, associated with the breakdown of actinolite, albite, epidote and chlorite. However, there are a number of important features of the Flin Flon sequence that are not reproduced within the modelling that affect interpretations of the devolatilization across this important interval including: (1)the lack of observed reaction progress and devolatilization within the hornblende-actinolite zone; (2) the considerable observed reaction progress including chlorite breakdown within the hornblende-actinolite-oligoclase zone; (3) the lack of a modal decrease in epidote proportions; (4) greater observed total amounts of chlorite breakdown across the greenschist-amphibolite facies transition zone. The final point is particularly important when evaluating the devolatilization evolution and particularly the possible fluid compositions across the greenschist-amphibolite facies transition zone, as discussed in the following section.

Determining whether differences in the thermodynamic predictions and natural observations stem from limitations with the modelling or whether they reflect real deviations from equilibrium behaviour is difficult. Modelling the greenschist-amphibolite facies transition zone is particularly problematic due to the key mineralogical changes involving phases within the same mineral group coexisting across miscibility gaps (i.e. actinolite-hornblende and albite-oligoclase miscibility gaps). This is particularly an issue for modelling plagioclase group minerals, for which no a-X model exists for predicting two coexisting plagioclase group minerals. Rather, the coexistence of albite and oligoclase is modelled with a 'solid-solution' oligoclase phase (Holland and Powell, 2003) coexisting with end-member albite (e.g. Dale et al., 2005; Elmer et al., 2006).

A number of features across the greenschist-amphibolite facies transition zone within Flin Flon are interpreted as being disequilibrium features, as discussed in detail in Starr and Pattison (2019). Their study concluded that the limited breakdown of epidote across the transition zone and the persistence of actinolite and albite a considerable distance up-grade of the oligoclase-in isograd likely resulted from the metastable persistence of these minerals as a result of the sluggish dissolution kinetics of epidote, albite and actinolite.

8.4. Comparison of predicted versus observed compositions of fluid release across the greenschist-amphibolite facies transition

T-XCO_2 modelling and the calculation of fluid buffering paths was used to predict the XCO_2 compositions of fluid released at different intervals across the greenschist-amphibolite facies transition. Observations from natural sequences such as at Flin Flon can be used to qualitatively assess fluid compositions by considering the effect of the breakdown of important accessory phases such as carbonate and sulphide minerals across devolatilization intervals.

The predicted XCO_2 composition of the fluid produced as a result of reactions involving the appearance of hornblende (point 1; Figs. 10, 11) and oligoclase (point 2; Figs. 10, 11) is limited to low XCO_2 values. Fluid buffer path modelling predicts that the XCO_2 content of fluid produced at the model equivalent of the hornblende-in isograd (point 1; Figs. 10) for the high-Mg basaltic composition may vary between 0.02 and 0.03 (based on mineral assemblage constraints), with a value of 0.02 predicted for both the average and maximum carbonate buffering paths (Fig. 10). The predicted XCO_2 values for the oligoclase-producing reaction (point 2; Figs. 10) have a maximum range of 0.02–0.08, and predicted values of 0.025 and 0.04 for the average and maximum carbonate buffering path respectively (Fig. 10). These values are very similar ($\pm$0.01) for modelling of the average high-Ca basaltic composition.

The lack of carbonate consumption predicted across these devolatilization intervals, and the resulting low XCO_2 fluid compositions (points 1 and 2; Figs. 10, 11), agree with petrographic and modal observations from the Flin Flon sequence that show no discernable change in the carbonate modal proportions within the hornblende-actinolite and hornblende-actinolite-oligoclase zones.

As discussed previously, there is no evidence for the breakdown of pyrite or any other sulphide phase across the hornblende-in or oligoclase-in isograds. This observation is potentially important because pyrite is the most likely host mineral for gold (e.g. Pitcairn et al., 2006, 2010, 2015; Tomkins, 2010), as well as the most likely source for the sulphur that is thought to complex with gold in orogenic gold fluids. The lack of evidence for change in the sulphide mineralogy at Flin Flon contrasts with observations from pelitic sequences that show a change in sulphide mineralogy between greenschist facies assemblages, which are dominated by pyrite, and amphibolite facies assemblages, in which this pyrite appears to have been replaced by pyrrhotite (e.g. Pitcairn et al., 2006, 2010, 2015). We note that the volume of sulphides in the Flin Flon metabasic rocks is lower than commonly reported in metapelites (e.g. Tomkins, 2010), and that their distribution is more heterogeneous, often occurring in veins. Given the difficulties of accurately determining prograde sulphide modal changes within the metabasites at Flin Flon as described previously, it is unclear whether small changes in the sulphide modal proportions would be resolvable.

Above the main greenschist-amphibolite facies transition, at grades higher than those observed at Flin Flon, the T-XCO_2 modelling predicts that fluid compositions are buffered to higher XCO_2 values (>0.1) within the Cal-Hbl-Chl-Ep-Pl or Cal-Hbl-Ep-Pl stability fields where chlorite, epidote and carbonate are predicted to react out of the rock. However, this does not implicate volumetrically significant fluid release with high XCO_2 values, because this is dependent upon the persistence of significant amounts of hydrous minerals (predominantly chlorite) and carbonate to temperatures above the main greenschist-amphibolite facies transition zone.

The modelling suggests that the ability of metabasalts to generate significant volumes of higher XCO_2 fluids (>0.1) is dependent on a number of factors, most importantly the abundance of carbonate minerals and the bulk composition of the silicate component of the metabasic rocks (Elmer et al., 2006; this study). For fluid buffering paths in rocks that have high carbonate contents (e.g. the maximum carbonate content observed in the Flin Flon sequence) (Fig. 10a, c; Figs. 11a, c), the fluid compositions are buffered to higher XCO_2 than those for the average carbonate contents, and are predicted to retain sufficient chlorite that, upon reaction, produces significant volumes of fluid with moderate XCO_2 values (0.2–0.3) (reaction 4; Fig. 10a, c; Figs. 11a, c). However, for the average carbonate or carbonate free systems (Fig. 10a, b, d; Figs. 11a, b, d), where most of the chlorite is predicted to react out at lower grade, there is minimal fluid release associated with reaction in these fields (reaction 4) and thus little fluid release with XCO_2 contents above 0.1.

Comparison of the T-XCO_2 modelling for the high-Mg and high-Ca bulk compositions, representing the pillow rim and core compositions, suggests that the bulk composition of the silicate component of the metabasites also plays an important role in controlling the fluid compositions. For the high-Ca composition, chlorite is lost at relatively low temperatures prior to loss of a significant portion of the calcite (Fig. 11). Thus for a high-Ca composition, whilst the fluids may be buffered to higher XCO_2 contents up-grade, the loss of chlorite at lower temperatures reduces the potential for significant fluid volumes with these higher XCO_2 compositions.

Petrological observations from the Flin Flon sequence that bear on the applicability of these modelling predictions include the loss of the majority of the chlorite at the greenschist-amphibolite facies transition

Table 1
Average and range of H_2O contents for greenschist and amphibolite facies samples estimated from petrological observations and thermodynamic modelling. 'Petro': H_2O contents estimated combining modal and compositional data of hydrous minerals. No values exist for the high-Na type due to insufficient data. Note that the petrological estimates for amphibolite facies conditions use only samples either from the upper part of the hornblende-actinolite-oligoclase zone or the hornblende-oligoclase zone, as these are most representative of amphibolite facies samples. 'Model': estimated using the bulk compositional modelling described in the text. Hacker (03): Hacker et al. (2003) – average H_2O content for metabasites of MORB composition at greenschist and amphibolite facies conditions calculated using a compilation of modal data. Dehydration wt%: Equal to the difference in hydrous content between the average greenschist and amphibolite facies values.

Bulk composition	H_2O wt% - GS facies average	H_2O wt% - GS facies range	H_2O wt% - amp facies average	H_2O wt% - amp facies range	Dehydration wt% average
High-Mg Type - Petro	3.1	2.1–3.7	1.3	1.2–1.4	1.8
High-Mg Type - Model	3.5	2.8–3.9	1.3	1.1–1.5	2.2
High-Ca Type - Petro	2.8	2.2–3.7	1.7	1.4–2.0	1.1
High-Ca Type - Model	3.1	2.4–3.6	1.3	1.1–1.7	1.8
High-Na Type - Petro	1.7	0.8–2.5	–	–	–
High-Na Type - Model	1.6	0.6–2.2	0.7	0.3–1.0	0.9
Hacker(03) - MORB Compilation	3.3	–	1.3	–	2.0

just above the oligoclase-in isograd, the generally low modal abundance of carbonate in this sequence, and the lack of evidence for its consumption going up-grade. As discussed previously, modal analysis and petrographic observations suggest the breakdown of the majority (>75%) of the chlorite within the hornblende-actinolite-oligoclase zone (Fig. 5; Fig. 10e, f; Fig. 11e, f), considerably more than predicted by the thermodynamic modelling. The low proportions of chlorite remaining (average: 4%) limits the amount of fluid that could have been released above the main greenschist-amphibolite facies transition zone, even if some equivalent of the thermodynamically predicted reactions at higher grades could have occurred. The combination of the modelling with observations from Flin Flon imply that significant production of fluids with XCO_2 compositions > 0.1 is unlikely to have occurred at Flin Flon.

8.5. Evaluating metabasites as the source of fluids for orogenic gold deposit formation

The above results suggest that the greenschist-amphibolite facies transition zone in metabasites represents a major interval of devolatilization, associated with the breakdown of the majority of the chlorite and mineral-bound water. However, these observations at Flin Flon also suggest that this devolatilization does not coincide with intervals of carbonate and pyrite breakdown that are thought to be important for generating fluids associated with orogenic gold deposits. The results suggest fluids released over the main greenschist-amphibolite facies transition zone are likely to have low XCO_2 compositions (<0.1), and that significant volumes of fluids with higher XCO_2 compositions (>0.2) are unlikely to be produced. Likewise, there is no evidence for the breakdown of pyrite across the devolatilization interval that would be the main source for the gold hydrosulphide complexes that are crucial for the transport of gold. These combined observations suggest that the fluids released across the greenschist-amphibolite facies transition at Flin Flon are unlikely to have the expected fluid composition of a potential source fluid for orogenic gold formation.

It is important to consider whether the observations from the Flin Flon Greenstone Belt are broadly applicable to other greenstone belts. The Flin Flon sequence appears to be a typical example of mafic crust undergoing burial metamorphism as part of a greenstone belt, with normal bulk compositions (see comparison in Fig. 3) and the typical sequence of mineral isograds and P-T conditions for Barrovian style metamorphism (e.g. Bégin, 1992; Liou et al., 1974; Starr and Pattison, 2019). However, an important variable, as noted by Elmer et al. (2006), is that oceanic basaltic sequences may undergo different degrees of carbonation. This controls the later metamorphic fluid signature, as shown above, and it is thus possible that this segment of the Flin Flon Greenstone Belt may represent a relatively uncarbonated segment of oceanic crust. The amount of carbonate within a sample at greenschist or lower amphibolite facies is dependent upon the initial carbonation associated with pre-metamorphic hydrothermal alteration and the degree to which the carbonate is consumed downgrade of the greenschist-amphibolite facies transition zone. Whilst there is textural evidence that small modal amounts of carbonate are stable at greenschist and lower amphibolite facies at Flin Flon, comparison of carbonate contents at prehnite-pumpellyite facies versus greenschist facies conditions suggests that there is carbonate loss in the prehnite-pumpellyite to greenschist facies transition (Starr et al., in review). This is consistent with the general observation that rocks within the prehnite-pumpellyite facies tend to retain significant igneous and hydrothermal mineralogy whereas greenschist facies samples are usually completely overprinted by metamorphic assemblages (Starr et al., in review). If the loss of carbonate at lower grades is a common feature of greenstone belts, it is possible that the low carbonate contents within greenschist and amphibolite facies rocks at Flin Flon, and the resulting low-XCO_2 compositions released across this interval, are typical even in sequences that may have undergone extensive sea floor carbonation.

In addition, the observations from Flin Flon suggest that, in contrast to thermodynamic modelling predictions, the majority of devolatilization occurs going through the greenschist-amphibolite facies transition zone associated with chlorite consumption, with little chlorite remaining for further dehydration. Modelling predictions and observations from Flin Flon suggest that the fluid released across this interval is limited to low XCO_2 compositions (<0.08) regardless of the carbonate content. If the lack of overlap between the major dehydration intervals resulting from chlorite consumption and the decarbonation interval(s) resulting from carbonate consumption is true of other sequences, the greenschist-amphibolite facies transition zone in metabasites may, as a general rule, be dominated volumetrically by fluids with low XCO_2 compositions. Further study of other natural sequences is required to test this hypothesis.

9. Conclusions

1. Documentation of mineral modes, compositions and textures indicate that the mineralogical transformation from greenschist facies to amphibolite facies in Flin Flon occurs predominantly within the relatively narrow hornblende-actinolite-oligoclase zone where there is significant devolatilization associated with the breakdown of ~75% of the total chlorite content. By contrast little reaction progress (and hence devolatilization) is seen within the lower-grade hornblende-actinolite zone.
2. The majority of samples contain calcite in low modal abundance (average modal proportion: 1.5%). There is no modal or textural evidence for the breakdown of carbonate minerals across the greenschist-amphibolite facies transition zone. Sulphide minerals, including pyrite, chalcopyrite, and pyrrhotite are present in very low proportions (<0.5%). No modal or textural evidence was documented for the breakdown of any sulphide phase (e.g. pyrite) within the Flin Flon sequence.

3. Observations from Flin Flon, combined with thermodynamic modelling, suggests that the amount of devolatilization is strongly controlled by variations in the bulk composition of the metabasites, the latter interpreted to result from pre-metamorphic alteration processes. Comparison of modelling and petrological estimates of the total devolatilization suggests that the modelling slightly overestimates the amount of fluid released. High-Mg and high-Ca basalts, representative of pillow rim and core material, undergo an average of 1.8 wt% (modelling estimate: 2.2 wt%) and 1.1 wt% (modelling estimate: 1.8 wt%) H_2O loss respectively.
4. T-XCO_2 phase diagram modelling, combined with the calculation of fluid buffering paths for varying carbonate contents predict that the Flin Flon sequence would predominantly produce fluids with low XCO_2 compositions (<0.08), for the hornblende and oligoclase-producing reactions, across the greenschist-amphibolite facies transition zone. These modelling predictions are consistent with natural observations from Flin Flon that indicate a lack of carbonate breakdown across the hornblende-actinolite and hornblende-actinolite-oligoclase zones.
5. A number of natural observations from the Flin Flon sequence differ from the modelling predictions including the lack of observed reaction progress and devolatilization within the hornblende-actinolite zone, the lack of a decrease in the epidote modal proportions, and the considerable devolatilization resulting from the breakdown of ~75% of the chlorite across the hornblende-actinolite-oligoclase zone. These differences are interpreted to reflect both limitations in the thermodynamic modelling and departures from equilibrium behaviour.
6. Fluid buffering path modelling predicts that fluid compositions may be buffered to higher XCO_2 values (>0.1) at higher grades above the main greenschist-amphibolite facies transition zone for samples with higher carbonate contents. However, several observations from the Flin Flon sequence suggest that the volume of such fluids produced at higher grades is limited. The breakdown of the majority of the chlorite (>75%) across the greenschist-amphibolite facies transition zone suggests there is little remaining chlorite (average modal proportions: 4%) to cause significant devolatilization at higher grades. In addition, the modelling suggests that the release of fluid with high-CO_2 compositions is limited to samples that contain high carbonate contents (>5%), which represents a small subset of those within the Flin Flon sequence.
7. Modal and textural observations suggests that there is only minor consumption of epidote across the transition zone, interpreted to be due to metastable persistence owing to sluggish dissolution kinetics. The breakdown of this epidote must result in a smaller devolatilization event at higher grades than exposed at Flin Flon though the nature of this event is difficult to characterise.
8. These observations, coupled with predictions from thermodynamic modelling, suggest that the greenschist-amphibolite facies transition zone in metabasites is associated with significant devolatilization over a small spatial and thermal interval but may not coincide with intervals of carbonate and pyrite breakdown. In this case, it is unlikely that fluids produced from metabasites across the greenschist-amphibolite facies transition zone would acquire the gold hydrosulphide ($Au(HS)_2^-$) complexes and moderate XCO_2 fluid compositions that are associated with orogenic gold fluids.

Acknowledgements

R. Marr is thanked for assistance with the electron microprobe at the University of Calgary. We also thank D.E. Ames and S.G. Digel for giving access to samples from the Flin Flon field area. We thank Richard Palin and Johann Diener for their insightful reviews and Marco Scambelluri for handling the manuscript. This research was supported by NSERC Discovery Grant 037233 to Pattison.

Appendix A. Supplementary data

Supplementary data to this article can be found online at https://doi.org/10.1016/j.lithos.2019.05.020.

References

Ames, D.E., Tardif, N., Maclachlan, K., Gibson, H.L., 2002. Geology and hydrothermal alteration of the flin Flon – Triple 7 – callinan VMS horizon hanging-wall stratigraphy: flin flon targeted geoscience initiative. summary of investigations 2002, volume 2 Sask. Ind. Res. 2, 1–12.

Ames, D.E., Kjarsgaard, I.M., Stirling, J.A.R., 2011. Mineral chemistry and x-ray diffraction database of greenschist- to amphibolite-facies assemblages in the hidden and louis formations, paleoproterozoic flin flon domain. Geol. Surv. Canada (Open File 6548).

Ames, D.E., Galley, A.G., Kjarsgaard, I.M., Tardif, N., Taylor, B.T., 2016. Hanging-wall vectoring for buried volcanogenic massive sulfide deposits, paleoproterozoic Flin Flon mining camp, Manitoba, Canada. Econ. Geol. 111, 963–1000.

Ashton, K.E., Heaman, L.M., Lewry, J.F., Hartlaub, R.P., Shi, R., 1999. Age and origin of the Jan Lake complex: a glimpse at the buried Archean craton of the Trans-Hudson Orogen. Can. J. Earth Sci. 36, 185–208.

Ashton, K.E., Lewry, J.F., Heaman, L.M., Hartlaub, R.P., Stauffer, M.R., Tran, H.T., 2005. The Pelican Thrust Zone: basal detachment between the Archean Sask Craton and Paleoproterozoic Flin Flon - Glennie Complex, western Trans-Hudson Orogen. Can. J. Earth Sci. 42, 685–706.

Bach, W., Hegner, E., Erzinger, J., Satir, M., 1994. Chemical and isotopic variations along the superfast spreading East Pacific Rise from 6 to 30°S. Contrib. Mineral. Petrol. 116, 365–380.

Bégin, N.J., 1992. Contrasting mineral isograd sequences in metabasites of the Cape Smith Belt, northern Québec, Canada: three new bathograds for mafic rocks. J. Metamorph. Geol. 10, 685–704.

Bickford, M.E., Collerson, K.D., Lewry, J.F., Van Schmus, W.R., Chiarenzelli, J.R., 1990. Proterozoic collisional tectonism in the Trans-Hudson orogen, Saskatchewan. Geology 18, 14–18.

Cann, J.R., 1969. Spilites from the Carlsberg Ridge, Indian Ocean. J. Petrol. 10, 1–19.

Coggon, R., Holland, T.J.B., 2002. Mixing properties of phengitic micas and revised garnet-phengite thermobarometers. J. Metamorph. Geol. 20, 683–696.

Dale, J., Powell, R., White, R.W., Elmer, F.L., Holland, T.J.B., 2005. A thermodynamic model for Ca–Na clinoamphiboles in Na_2O–CaO–FeO–MgO–Al_2O_3–SiO_2–H_2O–O for petrological calculations. J. Metamorph. Geol. 23, 771–791.

de Capitani, C., Brown, T.H., 1987. The computation of chemical equilibrium in complex systems containing non-ideal solutions. Geochim. Cosmochim. Acta 51, 2639–2652.

De Capitani, C., Petrakakis, K., 2010. The computation of equilibrium assemblage diagrams with Theriak/Domino software. Am. Mineral. 95, 1006–1016.

Dewolfe, Y.M., Gibson, H.L., 2006. Stratigraphic subdivision of the Hidden and Louis formations, Flin Flon, Manitoba (NTS 63K16SW). Report of Activities 2006, Manitoba Science, Technology, energy and mines. Manitoba Geol. Surv. 22–34.

DeWolfe, Y.M., Gibson, H.L., Lafrance, B., Bailes, A.H., 2009. Volcanic reconstruction of Paleoproterozoic arc volcanoes: the Hidden and Louis formations, Flin Flon, Manitoba, Canada. Can. J. Earth Sci. 46, 481–508.

Diener, J.F.A., Powell, R., 2010. Influence of ferric iron on the stability of mineral assemblages. J. Metamorph. Geol. 28, 599–613.

Diener, J.F.A., Powell, R., 2012. Revised activity-composition models for clinopyroxene and amphibole. J. Metamorph. Geol. 30, 131–142.

Diener, J.F.A., Powell, R., White, R.W., Holland, T.J.B., 2007. A new thermodynamic model for clino- and orthoamphiboles in the system Na_2O-CaO-FeO-MgO-Al_2O_3-SiO_2 -H_2O-O. J. Metamorph. Geol. 25, 631–656.

Elmer, F.L., White, R.W., Powell, R., 2006. Devolatilization of metabasic rocks during greenschist-amphibolite facies metamorphism. J. Metamorph. Geol. 24, 497–513.

Evans, K.A., Powell, R., Holland, T.J.B., 2010. Internally consistent data for Sulphur-bearing phases and application to the construction of pseudosections for mafic greenschist facies rocks in Na_2O-CaO-K_2O-FeO-MgO-Al_2O_3-SiO_2-CO_2-O-S-H_2O. J. Metamorph. Geol. 28, 667–687.

Fedorowich, J.S., Kerrich, R., Stauffer, M.R., 1995. Geodynamic evolution and thermal history of the central Flin Flon Domain, Trans-Hudson Orogen: constraints from structural development, $^{40}Ar/^{39}Ar$, and stable isotope geothermometry. Tectonics 14, 472–503.

Ferry, J.M., 1981. Petrology of graphitic sulfide-rich schists from south-central Maine: an example of desulfidation during prograde regional metamorphism. Am. Mineral. 66, 908–931.

Gaboury, D., 2013. Does gold in orogenic deposits come from pyrite in deeply buried carbon-rich sediments?: insight from volatiles in fluid inclusions. Geology 41, 1207–1210.

Goldfarb, R.J., Groves, D.I., 2015. Orogenic gold: common or evolving fluid and metal sources through time. Lithos 233, 2–26.

Goldfarb, R.J., Baker, T., Dube, B., Groves, D.I., Hart, J.R., Gosselin, P., 2005. Distribution, character, and genesis of gold deposits in metamorphic terranes. Econ. Geol. 407–450 100th Anniversary Volume.

Green, E., Holland, T., Powell, R., 2007. An order-disorder model for omphacitic pyroxenes in the system jadeite-diopside-hedenbergite-acmite, with applications to eclogitic rocks. Am. Mineral. 92, 1181–1189.

Groves, D.I., Goldfarb, R.J., Gebre-Mariam, M., Hagemann, S.G., Robert, F., 1998. Orogenic gold deposits: a proposed classification in the context of their crustal distribution and relationship to other gold deposit types. Ore Geol. Rev. 13, 7–27.

Hacker, B.R., Abers, G.A., Peacock, S.M., 2003. Subduction factory 1. Theoretical mineralogy, densities, seismic wave speeds, and H2O contents. J. Geophys. Res. 108, 2029.
Hart, S.R., Erlank, A.J., Kable, E.J.D., 1974. Sea floor basalt alteration: some chemical and Sr isotopic effects. Contrib. Mineral. Petrol. 44, 219–230.
Herrmann, A.G., Potts, M.J., Knake, D., 1974. Geochemistry of the rare earth elements in Spilites from the oceanic and continental crust. Contrib. Mineral. Petrol. 44, 1–16.
Hoffman, P.F., 1988. United plates of America, the Birth of a Craton: early proterozoic assembly of laurentia. Annu. Rev. Earth Planet. Sci. 16, 543–603.
Holland, T.J.B., Powell, R., 1998. An internally consistent thermodynamic data set for phases of petrological interest. J. Metamorph. Geol. 16, 309–343.
Holland, T.J.B., Powell, R., 2003. Activity-composition relations for phases in petrological calculations: an asymetric multicomponent formulation. Contrib. Mineral. Petrol. 145, 492–501.
Holland, T.J.B., Baker, J.M., Powell, R., 1998. Mixing properties and activity- composition relationships of chlorites in the system MgO-FeO-Al_2O_3-SiO_2-H_2O. Eur. J. Mineral. 10, 395–406.
Humphris, S.E., Thompson, G., 1978. Hydrothermal alteration of oceanic basalts by seawater. Geochim. Cosmochim. Acta 42, 107–125.
Kerrich, R., Fyfe, W.S., 1981. The gold-carbonate association: source of CO_2, and CO_2 fixation reactions in archaean lode deposits. Chem. Geol. 33, 265–294.
Kretz, R., 1983. Symbols for rock-forming minerals. Am. Mineral. 68, 277–279.
Large, R.R., Bull, S.W., Maslennikov, V.V., 2011. A carbonaceous sedimentary source-rock model for carlin-type and orogenic gold deposits. Econ. Geol. 106, 331–358.
Liou, J.G., Kuniyoshi, S., Ito, K., 1974. Experimental studies of the phase relations between greenschist and amphibolite in a basaltic system. Am. J. Sci. 274, 613–632.
Lucas, S.B., Stern, R.A., Syme, E.C., Reilly, B.A., Thomas, D.J., 1996. Intraoceanic tectonics and the development of continental crust: 1.92-1.84 Ga evolution of the Flin Flon Belt, Canada. Geol. Soc. Am. Bull. 108, 602–629.
Mullen, E.D., 1983. MnO/TiO_2/P_2O_5: a minor element discriminant for basaltic rocks of oceanic environments and its implications for petrogenesis. Earth Planet. Sci. Lett. 62, 53–62.
Norton, D., Knapp, R., 1977. Transport phenomena in hydrothermal systems: the nature of porosity. Am. J. Sci. 277, 913–936.
Phillips, G.N., Evans, K.A., 2004. Role of CO_2 in the formation of gold deposits. Nature 429, 860–863.
Phillips, G.N., Powell, R., 2009. Formation of gold deposits: review and evaluation of the continuum model. Earth Sci. Rev. 94, 1–21.
Phillips, G.N., Powell, R., 2010. Formation of gold deposits: a metamorphic devolatilization model. J. Metamorph. Geol. 28, 689–718.
Phillips, G.N., Powell, R., 2011. Origin of Witwatersrand gold: a metamorphic devolatilisation–hydrothermal replacement model. Appl. Earth Sci. 120, 112–129.
Pitcairn, I.K., Teagle, D.A.H., Craw, D., Olivo, G.R., Kerrich, R., Brewer, T.S., 2006. Sources of metals and fluids in orogenic gold deposits: insights from the Otago and Alpine Schists, New Zealand. Econ. Geol. 101, 1525–1546.
Pitcairn, I.K., Olivo, G.R., Teagle, D.A.H., Craw, D., 2010. Sulfide evolution during Prograde Metamorphism of the Otago and Alpine Schists, New Zealand. Can. Mineral. 48, 1267–1295.
Pitcairn, I.K., Skelton, A.D.L., Wohlgemuth-Ueberwasser, C.C., 2015. Mobility of gold during metamorphism of the Dalradian in Scotland. Lithos 233, 69–88.
Polat, A., Hofmann, A.W., Münker, C., Regelous, M., Appel, P.W.U., 2003. Contrasting geochemical patterns in the 3.7-3.8 Ga pillow basalt cores and rims, Isua greenstone belt, Southwest Greenland: Implications for postmagmatic alteration processes. Geochim. Cosmochim. Acta 67, 441–457.
Polat, A., Appel, P.W.U., Frei, R., Pan, Y., Dilek, Y., Ordóñez-Calderón, J.C., Fryer, B., Hollis, J.A., Raith, J.G., 2007. Field and geochemical characteristics of the Mesoarchean (~3075 Ma) Ivisaartoq greenstone belt, southern West Greenland: evidence for seafloor hydrothermal alteration in supra-subduction oceanic crust. Gondwana Res. 11, 69–91.
Powell, R., Will, T.M., Phillips, G.N., 1991. Metamorphism in Archaean greenstone belts: calculated fluid compositions and implications for gold mineralization. J. Metamorph. Geol. 9, 141–150.
Rebay, G., Powell, R., Diener, J.F.A., 2010. Calculated phase equilibria for a MORB composition in a P-T range, 450-650°C and 18-28 kbar: the stability of eclogite. J. Metamorph. Geol. 28, 635–645.
Richardson, C.J., Cann, J.R., Richards, H.G., Cowan, J.G., 1987. Metal-depleted root zones of the Troodos ore-forming hydrothermal systems, Cyprus. Earth Planet. Sci. Lett. 84, 243–253.
Ridley, J.R., Diamond, L.W., 2000. Fluid chemistry of orogenic lode gold deposits and implications for genetic models. Rev. Econ. Geol. 13, 141–162.
Schilling, J.G., Zajac, M., Evans, R., Johnston, T., White, W., Devine, J.D., Kingsley, R., 1983. Petrologic and geochemical variations along the Mid-Atlantic Ridge from 29°N to 73°N. Am. J. Sci. 283, 510–586.
Seyfried, W.E., Mottl, M.J., Bischoff, J.L., 1978. Seawater/basalt ratio effects on the chemistry and mineralogy of spilites from the ocean floor. Nature 275, 211–213.
Starr, P.G., Pattison, D.R.M., 2019. Equilibrium and disequilibrium processes across the greenschist – amphibolite transition zone in metabasites. Contrib. Mineral. Petrol. 174.
Stauffer, M.R., 1984. Manikewan: an early proterozoic ocean in Central Canada, its igneous history and orogenic closure. Precambrian Res. 25, 257–281.
Stern, R.A., Syme, E.C., Bailes, A.H., Lucas, S.B., 1995. Paleoproterozoic (1.90-1.86 Ga) arc volcanism in the Flin Flon Belt, Trans-Hudson Orogen, Canada. Contrib. Mineral. Petrol. 119, 117–141.
Sun, S.-S., McDonough, W.F., 1989. Chemical and isotopic systematics of oceanic basalts: implications for mantle composition and processes. Geol. Soc. Spec. Publ. 42, 313–345.
Syme, E.C., Lucas, S.B., Bailes, A.H., Stern, R.A., 1999. Contrasting arc and MORB-like assemblages in the Paleoproterozoic Flin Flon Belt, Manitoba, and the role of intra-arc extension in localizing volcanic-hosted massive sulphide deposits. Can. J. Earth Sci. 36, 1767–1788.
Teagle, D.A.H., Alt, J.C., 2004. Hydrothermal alteration of basalts beneath the bent hill massive sulfide deposit, Middle Valley, Juan de Fuca Ridge. Econ. Geol. 99, 561–584.
Tomkins, A.G., 2010. Windows of metamorphic sulfur liberation in the crust : implications for gold deposit genesis. Geochim. Cosmochim. Acta 74, 3246–3259.
Tomkins, A.G., 2013. On the source of orogenic gold. Geology 41, 1255–1256.
Vallance, T.G., 1965. On the chemistry of pillow lavas and the origin of spilites. Mineral. Mag. 34, 471–481.
Wang, J., Kusky, T.M., Polat, A., Wang, L., Peng, S., Jiang, X., Deng, H., Wang, S., 2012. Seafloor metamorphism recorded in epidosites from the ca. 1.0 Ga Miaowan Ophiolite, Huangling Aniticline, China. J. Earth Sci. 23, 696–704.
White, R.W., Powell, R., Holland, T.J.B., Worley, B., 2000. The effect of TiO_2 and Fe_2O_3 on metapelitic assemblages at greenschist and amphibolite facies conditions: mineral equilibria calculations in the system K_2O-FeO-MgO-Al_2O_3-SiO_2-H_2O-TiO_2-Fe_2O_3. J. Metamorph. Geol. 18, 497–511.
White, R.W., Powell, R., Clarke, G.L., 2002. The interpretation of reaction textures in Fe-rich metapelitic granulites of the Musgrave Block, Central Australia: Constraints from mineral equilibria calculations in the system. J. Metamorph. Geol. 20, 41–55.
White, R.W., Powell, R., Phillips, G.N., 2003. A mineral equilibria study of the hydrothermal alteration in mafic greenschist facies rocks at Kalgoorlie, Western Australia. J. Metamorph. Geol. 21, 455–468.
White, R.W., Pomroy, N.E., Powell, R., 2005. An in situ metatexite-diatexite transition in upper amphibolite facies rocks from Broken Hill, Australia. J. Metamorph. Geol. 23, 579–602.
White, R.W., Powell, R., Holland, T.J.B., 2007. Progress relating to calculation of partial melting equilibria for metapelites. J. Metamorph. Geol. 25, 511–527.
Widmer, T., Ganguin, J., Thompson, A.B., 2000. Ocean floor hydrothermal veins in eclogite facies rocks of the Zermatt-Saas Zone, Switzerland. Schweiz. Mineral. Petrogr. Mitt. 80, 63–73.
Xue, Y., Campbell, I., Ireland, T.R., Holden, P., Armstrong, R., 2013. No mass-independent sulfur isotope fractionation in auriferous fluids supports a magmatic origin for Archean gold deposits. Geology 41, 791–794.